

A Cu-only superoxide dismutase from stripe rust fungi functions as a virulence factor deployed for counter defense against host-derived oxidative stress

Peijing Zheng^{1†}, Liyang Chen^{1†}, Suye Zhong¹, Xiaobo Wei¹, Qi Zhao², Qinglin Pan³, Zhensheng Kang^{3*}, Jie Liu^{1*}

¹State Key Laboratory of Crop Stress Biology for Arid Areas and College of Life Sciences, Northwest A&F University, Yangling, 712100 Shaanxi, China

²State Key Laboratory of Crop Stress Biology for Arid Areas and College of Science, Northwest A&F University, Yangling, 712100 Shaanxi, China

³State Key Laboratory of Crop Stress Biology for Arid Areas and College of Plant Protection, Northwest A&F University, Yangling, 712100 Shaanxi, China

*For correspondence. E-mail: liujie2003@hotmail.com; Tel. (+86) 029-87092262; Fax. (+86) 029-87092262

E-mail: kangzs@nwsuaf.edu.cn; Tel. (+86) 02987080061; Fax (+86) 02987080061

[†]These authors contributed equally to this work.

A running title: Functional characterization of PsSOD2.

This article has been accepted for publication and undergone full peer review but has not been through the copyediting, typesetting, pagination and proofreading process which may lead to differences between this version and the Version of Record. Please cite this article as doi: 10.1111/1462-2920.15236

Summary

Plants quickly accumulate reactive oxygen species (ROS) to resist against pathogen invasion, while pathogens strive to escape host immune surveillance by degrading ROS. However, the nature of the strategies that fungal pathogens adopt to counteract host-derived oxidative stress is manifold, and requires deep investigation. In this study, a superoxide dismutase (SOD) from *Puccinia striiformis* f. sp. *tritici* (*Pst*) PsSOD2 with a signal peptide (SP) and the glycosylphosphatidylinositol (GPI) anchor, strongly induced during infection, was analysed for its biological characteristics and potential role in wheat-*Pst* interactions. The results showed that *PsSOD2* encodes a Cu-only SOD and responded to ROS treatment. Heterologous complementation assays in *Saccharomyces cerevisiae* suggest that the SP of PsSOD2 is functional for its secretion. Transient expression in *Nicotiana benthamiana* leaves revealed that PsSOD2 is localized to the plasma membrane. In addition, knockdown of *PsSOD2* by host induced gene silencing (HIGS) reduced *Pst* virulence and resulted in restricted hyphal development and increased ROS accumulation. In contrast, heterologous transient assays of *PsSOD2* suppressed flg22-elicited ROS production. Taken together, our data indicate that PsSOD2, as a virulence factor, was induced and localized to the plasma membrane where it may function to scavenge host-derived ROS for promoting fungal infection.

Introduction

Reactive oxygen species (ROS) are considered as by-products of aerobic metabolism, including superoxide anion ($O_2^{\bullet-}$), hydroxyl radical (HO^{\bullet}) and hydrogen peroxide (H_2O_2) (Mittler *et al.*, 2004). In plants, intracellular ROS are generated in organelles such as chloroplasts, mitochondria and peroxisomes, whereas extracellular ROS are produced by plasma membrane-localized NADPH oxidases, cell wall peroxidases and amine oxidases (Kadota *et al.* 2014; Kadota *et al.* 2015). Once plants are challenged by pathogens, ROS quickly accumulate and trigger a wide range of defense responses (i.e. programmed cell death, PCD) against pathogen invasion (Baxter *et al.* 2014). Additionally, these incompletely reduced oxygen species can directly lead to pathogen death through lipid and protein oxidation and nucleic acid degradation due to their inherent features (Apel and Hirt, 2004). Accordingly, pathogens can develop specified enzymes that respond to host's immunity defenses (Broxton and Culotta, 2016).

The antioxidative defense system consists of antioxidant enzymes such as superoxide dismutases (SODs), catalases (CATs), glutathione peroxidase, glutathione S-transferases and ascorbate-glutathione cycle enzymes and non-enzymatic antioxidants such as glutathione, thioredoxins and cupredoxins (Blokhina *et al.*, 2003; Staerck *et al.*, 2017). SODs are the first and most important defense line against oxidative stress that catalyze the dismutation of superoxide anions to hydrogen peroxide and molecular oxygen (Fridovich, 1995). They are ubiquitous to all

Accepted Article

forms of life and present in diverse locations in different organisms. SODs are expressed in prokaryotes, mitochondria, peroxisome, chloroplasts, cytosol and extracellular milieu of eukaryotes (Zeinali *et al.*, 2015). Presently, SODs are divided into three distinct families based on the type of metal ions that support activity: copper/zinc SOD (Cu/Zn-SOD), iron/manganese SOD (Fe/Mn-SOD) and nickel SOD (Ni-SOD) (Miller, 2012). Although these enzymes carry out the same function, they show significant differences in crystal structures, utilization of metal cofactors and catalytic mechanism (Zelko *et al.*, 2002). Of these, Cu/Zn-SOD and Fe/Mn-SOD are deemed to play a key role in protection against oxidative stress (Lu *et al.*, 2015). Cu/Zn-SOD, the first identified SOD, shares a signature motif related to the active site (Mccord and Fridovich, 1969). In general, Cu/Zn-SOD is homodimeric and exhibits diverse subcellular distributions in different organisms (Bafana *et al.*, 2010). While Fe/Mn-SOD is typically homodimers or homotetramers and commonly requires either Mn^{2+} or Fe^{2+} to perform its biological activity (Jackson and Brunold, 2004). The expression of major SOD isoforms is regulated by various stress treatments (Pilon *et al.*, 2011). Ni-SOD is restricted to few groups of organisms and has only been discovered in streptomycetes (Youn *et al.*, 1996), actinobacteria (Schmidt *et al.*, 2009), cyanobacteria (Eitinger, 2004) and algae (so far) (Morrissey and Bowler, 2012).

As with other eukaryotes, fungi mainly express cytosolic Cu/Zn-SODs and mitochondrial Mn-SODs (Bafana *et al.*, 2010). Some SODs have proven to correlate with fungal cell differentiation, virulence and stress resistance. For example, the inactivation of a fungal Cu/Zn-SOD resulted in reduced growth rates (Briones-Martindel-Campo *et al.*, 2015), disordered conidiation rhythm (Yoshida *et al.*, 2008) and impaired sporulation potential and mycorrhization (Abba *et al.*, 2009). The SOD1 (a cytosolic Cu/Zn-SOD)-disrupted mutant of *Candida albicans* exhibits attenuated virulence in an animal model of systemic infection (Hwang *et al.*, 2002). Similarly, a mitochondrial Mn-SOD-null mutant of *Aspergillus fumigatus* could not grow under thermal and oxidative stresses (Lambou *et al.*, 2010). O'Brien *et al.* (2004) found that a

Schizosaccharomyces cerevisiae Mn-SOD knockout became more susceptible to endogenous oxidative stress. In addition, a mitochondrial Mn-SOD BbSOD3 is required for *Beauveria bassiana* virulence and stress responses (Xie *et al.*, 2012). The *sod2* mutant of *Cryptococcus neoformans* (defective for a mitochondrial Mn-SOD) was avirulent in intranasally infected mice and markedly reduced in its virulence in intravenously infected mice. The virulence defect of *sod2* mutant appeared related to its growth defects in high oxygen environment (Narasipura *et al.*, 2005).

In addition to intracellular SODs, some fungal pathogens express extracellular SODs (EC-SODs) that seem tailor-made for host invasion. Fungal EC-SODs are the predominant antioxidant enzyme secreted into the extracellular space during infection. They are either secreted outside cells or attached to the cell wall by a glycosylphosphatidylinositol (GPI) anchor with a putative omega site at specific residues (Gleason *et al.*, 2014). Numerous studies have indicated that EC-SODs are essential for pathogen virulence during infection of host. For example, the fungal pathogen *Histoplasma capsulatum* secretes EC-SOD SOD3 to promote pathogenesis by removing host-derived ROS (Youseff *et al.*, 2012). In *C. albicans*, three EC-SODs (Sod4, Sod5, and Sod6) are adhered to the cell wall through GPI anchors (Frohner *et al.*, 2009). Of these, Sod5 has been well characterized and is confirmed to directly scavenge host-derived superoxide and to facilitate virulence in animal models (Gleason *et al.*, 2014). *Puccinia striiformis* f. sp. *tritici* (*Pst*) secreted a Zn-only SOD, PsSOD1, into the host-pathogen interface to contribute to *Pst* infection by combating superoxide from the host cells (Liu *et al.*, 2016). Additionally, systemic mycosis pathogen *Paracoccidioides brasiliensis* expresses an EC-SOD, PbSOD3, to counteract the oxidative burst of immune cells (Tamayo *et al.*, 2016).

Wheat stripe rust, caused by the obligate biotrophic fungus *Pst*, can result in serious wheat yield losses. *Pst* invasion induces host immunity and is accompanied by ROS accumulation at the plant-pathogen interface (Wang *et al.*, 2007). However, the molecular mechanisms by which *Pst*

Accepted Article

scavenges host-derived ROS remains unclear. In this study, a Cu-only SOD gene (*PsSOD2*) that responds to ROS was significantly up-regulated during *Pst* infection of wheat. Secretion and biochemical characteristics of PsSOD2 were determined by heterologous expression. PsSOD2 was localized to the plasma membrane, which is dependent on the GPI anchor. In addition, the function of *PsSOD2* was identified through overexpression and host induced gene silencing (HIGS). Our results indicate that PsSOD2 served as a virulence factor to promote *Pst* infection of wheat by counteracting host-derived oxidative stress.

Results

Each rust fungus only contains an EC-SOD with the GPI anchor

The genomes of *Puccinia striiformis*, *Puccinia graminis*, *Puccinia triticina*, *Puccinia sorghi* and *Melampsora larici-populina* were analyzed and all SODs in each genome were obtained. The signal peptides (SPs) and GPI anchors of the SODs were then predicted. The results showed that the obtained SODs contain a high proportion of EC-SODs in each rust fungus (Supporting Information Table S1). Interestingly, each rust fungus only has an EC-SOD containing the GPI anchor (Supporting Information Table S1). To elucidate the function of this kind of SODs, the SOD gene from *Pst*, *PsSOD2*, different from another identified SOD gene *PsSOD1* (Liu *et al.*, 2016), was chosen for further study.

PsSOD2 likely encodes a Cu-only SOD

PsSOD2 was amplified by RT-PCR using a CYR32-infected Suwon 11 (Su11) cDNA sample as a template. The open reading frame (ORF) of *PsSOD2* consists of 576 nucleotides and is predicted to encode a polypeptide of 191 amino acids with a calculated molecular mass of 19,791 Da, an isoelectric point (pI) of 9.23, and a Cu/Zn-SOD domain. Interestingly, similar to reported SOD4, SOD5 and SOD6 from *C. albicans* (Gleason *et al.*, 2014), PsSOD2 only contains Cu²⁺ binding sites (H86, H88, H104, and H168) and the disulfide cysteines (C98 and C177), but missed ligands for zinc and the electrostatic loop region (Supporting Information Fig. S1A and B), indicating that PsSOD2 is possibly a Cu-only SOD enzyme. In addition, SP and GPI-anchor prediction revealed

that PsSOD2 is likely a secreted protein anchored to plasma membrane and/or cell wall (Supporting Information Fig. S2A and B). It should be pointed out that the other four EC-SODs with the GPI anchor from *P. graminis*, *P. triticina*, *P. sorghi* and *M. larici-populina* also share similar characteristics (only containing Cu²⁺ binding sites) with PsSOD2 (data not shown).

The 203 amino acid sequence of PsSOD2 was used as a BLAST query sequence against the NCBI non-redundant protein sequence databases. The phylogenetic analysis revealed that PsSOD2 shows a closer relationship to Cu/Zn-SODs from basidiomycetes, particularly rust fungi, compared with those from ascomycetes (Supporting Information Fig. S3). PsSOD2 exhibited the highest sequence identity (57.46%) with the Cu/Zn-SOD from *P. sorghi* (GenBank accession number KNZ50864.1, Supporting Information Fig. S3).

***PsSOD2* is highly conserved between *Pst* isolates**

To determine intraspecies polymorphisms in *PsSOD2*, the coding regions of *PsSOD2* from five sequenced *Pst* isolates including a Chinese isolate (CYR32), three US isolates (PST21, PST08/21 and PST43) and a UK isolate (PST87-7), were compared. Compared with the *PsSOD2* sequence from CYR32, only five nucleotide substitutions were observed among the five *Pst* isolates, including one synonymous substitution and four non-synonymous substitutions (Supporting Information Table S2). In addition, the four mutations are not in the SOD domain or the Cu²⁺ binding sites of PsSOD2 (Supporting Information Fig. S4). Thus, the amino acid sequences of PsSOD2 are conserved between *Pst* isolates.

***PsSOD2* is induced possibly by host-derived ROS during *Pst* infection**

The expression pattern of *PsSOD2* was assayed at different stages of *Pst* infection by quantitative real-time PCR (qRT-PCR). The results showed that *PsSOD2* was expressed in ungerminated/germinated urediniospores and *Pst*-infected wheat tissues sampled from 6 to 264 hours post inoculation (hpi). Urediniospores germinated on water exhibited no difference in the *PsSOD2* transcript levels compared with ungerminated urediniospores (Fig. 1A). Once *Pst* was inoculated

on wheat leaves, the expression of *PsSOD2* was significantly up-regulated at 6 hpi and remained persistently high until 72 hpi (Fig. 1A). These results indicate an in-planta induction of *PsSOD2* during *Pst* infection.

To clarify whether up-regulation of *PsSOD2* was involved in ROS accumulated in wheat-*Pst* interactions, the construct pCB308-*PsSOD2np* (the β -glucuronidase (GUS) reporter gene is driven by the promoter of *PsSOD2*) was generated and transferred into *Nicotiana benthamiana* leaves by *A. tumefaciens*-mediated transformation. GUS activity was determined in infiltrated *N. benthamiana* leaves after H₂O₂ spraying. Our results show that H₂O₂ treatment caused an increase in reporter activity at 1 and 2 hpt (Fig. 1B). No significant changes were observed in the control (Fig. 1B). The GUS activity response to H₂O₂ treatment indicates *PsSOD2* expression is induced by ROS. Thus, we infer that up-regulation of *PsSOD2* during *Pst* infection is possibly due to host-derived ROS.

Enzymatic properties of PsSOD2

The recombinant His-tag PsSOD2 protein was expressed and purified by one-step chromatography. As shown in Fig. 2A and Supporting Information Fig. S5A, the fusion protein exhibited electrophoretic mobility of about 34 kDa on SDS-PAGE and identified by Western blotting (Supporting Information Fig. S5B). Enzymatic characteristics of PsSOD2 were then measured. The results showed that the optimum temperature of PsSOD2 was approximately 20°C and higher temperatures triggered a rapid fall of enzymatic activity (Fig. 2B). The optimum pH value of PsSOD2 was approximately 10 (Fig. 2C). In addition, the effects of metal cations on the enzymatic activity of PsSOD2 were also determined. Compared with enzymatic activity of PsSOD2 without addition of metal cations, inclusion of 0.5 mM Cu²⁺ in the reaction mixture enhanced PsSOD2 activity by 81% (Fig. 2D), whereas Zn²⁺, Mn²⁺ and Fe³⁺ produced no obvious influence on enzymatic activity (Fig. 2D). Also, removal of metal cations almost resulted in inactivity of PsSOD2, which may be recovered by supplement of Cu²⁺, but not Zn²⁺ (Supporting

Information Fig. S5C). These results indicate that PsSOD2 functions as a Cu-only SOD.

The PsSOD2 SP is functional

To validate the function of the PsSOD2 SP, the construct pSUC2-*PsSOD2*_{sp} was transformed into the invertase mutated yeast strain YTK12. pSUC2-*Mg87*₁₋₇₅ and the empty vector pSUC2 were the negative controls. pSUC2-*Avr1b*_{sp} served as a positive control. The results showed that two fusion constructs pSUC2-*PsSOD2*_{sp} and pSUC2-*Avr1b*_{sp} enabled YTK12 to grow on CMD-W media (yeast with invertase can grow) and YPRAA media (yeast with secreted invertase can grow) (Fig. 3A). However, pSUC2-*Mg87*₁₋₇₅ could not rescue yeast cell growth on YPRAA plates (Fig. 3A). The enzyme activity of secreted invertase was also detected by the 2,3,5-triphenyltetrazolium chloride (TTC) reaction. The results showed that the culture supernatants of the transformants containing pSUC2-*PsSOD2*_{sp} and pSUC2-*Avr1b*_{sp} (positive control) could cause red coloration of TTC, but the transformant containing pSUC2-*Mg87*₁₋₇₅ (negative control) and the empty vector not (Fig. 3B). These results confirmed that the SP of PsSOD2 is functional, which was consistent with the SignalP 4.1 predictions (Supporting Information Fig. S2A).

PsSOD2 is localized to the plasma membrane

To determine the subcellular localization of PsSOD2, the recombinant plasmids pK7FWG2-*PsSOD2*_{sp}:*GFP:PsSOD2*₈₅₋₅₇₆ and pK7FWG2-*PsSOD2*_{sp}:*GFP:PsSOD2*₈₅₋₅₀₇ were constructed (Fig. 4A). *Agrobacteria*-mediated transient expression in *N. benthamiana* leaves was carried out. GFP signal from the GFP-PsSOD2 fusion protein was exclusively found in the outer membrane ring after plasmolysis induced by 1 M sorbitol (Fig. 4B), indicating that PsSOD2 is localized to the plasma membrane. In contrast, GFP-PsSOD2_{ΔGPI} (a PsSOD2 mutant deleting the GPI anchor) proteins were secreted into the apoplast in tobacco leaves transformed by the pK7FWG2-*PsSOD2*_{sp}:*GFP:PsSOD2*₈₅₋₅₀₇ plasmid (Fig. 4C), suggesting that the plasma membrane localization of PsSOD2 required the GPI anchor

PsSOD2 suppressed ROS accumulation

In order to further identify the function of PsSOD2 in scavenging ROS, the recombinant plasmid pK7FWG2-*PsSOD2*_{sp}:*GFP:PsSOD2*₈₅₋₅₇₆ was transiently transformed into *N. benthamiana* leaves by agroinfiltration. After two days, leaf disks were punched and incubated in water. Flg22 (the active epitope of bacterial flagellin)-induced ROS burst in abovementioned leaf disks was then measured by luminol chemiluminescent reaction. The results showed that the ROS production was significantly decreased in the *PsSOD2* expressing *N. benthamiana* leaves compared with the GFP control (Fig. 5A), indicating that PsSOD2 could suppress ROS accumulation. The expression of the GFP-*PsSOD2* fusion protein was confirmed by Western blotting as shown in Fig. 5B.

Down-regulation of *PsSOD2* expression reduces *Pst* pathogenicity

To investigate the function of *PsSOD2* during *Pst* infection of wheat, the HIGS technique was employed to silence *PsSOD2* in *Pst*. Barly stripe mosaic virus (BSMV)-inoculated wheat seedlings exhibited mild chlorotic mosaic symptoms at 9 days after inoculation (dai), and no obvious growth defects were visualized (Fig. 6A). At 15 dai, a photo-bleaching phenotype in the *TaPDS* (*TaPDS*: wheat phytoene desaturase gene)-silenced wheat leaves indicated that the BSMV-HIGS system was functioning (Fig. 6A). The fourth leaves of BSMV-inoculated wheat plants were infected with CYR32, and the disease phenotypes were observed at 15 dai. On BSMV:*PsSOD2*-inoculated wheat leaves, fewer uredia were formed compared with the control (Fig. 6B). Additionally, the wheat plants inoculated with BSMV:*PsSOD2*-as1 (carrying a 161-bp fragment of *PsSOD2*, nucleotides 173–333) and BSMV:*PsSOD2*-as2 (carrying a 167-bp fragment of *PsSOD2*, nucleotides 332–498) displayed a similar disease phenotype, indicating that the silencing of *PsSOD2* was specific (Fig. 6B).

To determine whether decreased uredia production was due to restricted hyphal development, fungal biomass in the host tissue was measured as described by Liu *et al.* (2016). In *Pst*-infected wheat leaves inoculated with BSMV:*PsSOD2*-as1 and BSMV:*PsSOD2*-as2, the fungal biomass was obviously reduced by 20% and 21%, respectively, compared with the controls inoculated with

BSMV:γ (empty BSMV) (Fig. 6C). This result revealed that silencing of *PsSOD2* led to impeded fungal growth and reduction in sporulation.

To test whether *PsSOD2* was successfully silenced, the expression of *PsSOD2* was monitored using qRT-PCR in *Pst*-infected wheat leaves. The results showed that The *PsSOD2* transcript in BSMV:*PsSOD2*-as1-inoculated leaves was reduced by 67%, 48%, and 52% at 24, 48, and 120 hpi, respectively; in leaves inoculated with BSMV:*PsSOD2*-as2, the *PsSOD2* expression level was decreased by 86%, 74%, and 50%, respectively, compared with BSMV:γ-infected wheat leaves (Fig. 6D). These results indicate that the expression of *PsSOD2* was significantly knocked down via BSMV-HIGS.

HIGS of *PsSOD2* resulted in blocked fungal growth and enhanced ROS accumulation

To determine *PsSOD2* contribution to *Pst* pathogenicity, the fungal development and host response were detected in HIGS wheat plants infected with *Pst*. At 24 and 48 hpi, the number of hyphal branches, haustorial mother cells and haustoria in BSMV:*PsSOD2*-as1 or BSMV:*PsSOD2*-as2-inoculated wheat plants infected with *Pst* were similar ($P > 0.05$) to those of the control (Fig. 7K; Supporting Information Fig. S6A); however, hyphal length was obviously reduced (Fig. 7A, B, F, G and L; Supporting Information Fig. S6B). In addition, no significant difference was observed in the formation of secondary hyphae compared with the control at 24 and 48 hpi (Supporting Information Fig. S6C), while the infection area became smaller than the control at 120 hpi (Fig. 7C, H and M). To analyze the response of the host, H_2O_2 accumulation was assayed by DAB staining. The results revealed that H_2O_2 accumulation was significantly enhanced in the wheat plants inoculated with BSMV:*PsSOD2*-as1 and BSMV:*PsSOD2*-as2 compared with the control plants at 24 and 48 hpi (Fig. 7D, E, I, J and N; Supporting Information Fig. S6D).

Wheat heavy metal ATPase (HMA) genes were induced during *Pst* infection

Cu concentration at the wheat-*Pst* interface is pivotal for enzymatic activity of PsSOD2. In order

to clarify Cu transport in the wheat leaves infected by *Pst*, transcriptomic data of *HMA*s involved in Cu efflux from the cytoplasm and Cu transporter (COPT) genes acting in Cu homeostasis by Cu uptake were searched from the exp-VIP (<http://www.wheat-expression.com/>). The results showed that five HMA genes (TraesCS7A02G480100, TraesCS7B02G382300, TraesCS7D02G467100, TraesCS7B02G320100 and TraesCS2A02G162900) were induced (Fig. 8A). qRT-PCR analysis further confirmed that expression of TraesCS7B02G320100 (Fig. 8B), TraesCS2A02G162900 (Fig. 8C) and TraesCS7D02G467100 (allelic to TraesCS7A02G480100 and TraesCS7B02G382300; Fig. 8D) was up-regulated in *Pst*-infected wheat leaves. In contrast, no significant change was observed for COPT genes (Supporting Information Fig. S7).

Discussion

Although SODs are crucial in scavenging ROS, few studies regarding fungal SOD functions in counteracting host-derived oxidative stress are reported. In this study, the expression pattern of *PsSOD2* encoding a *Pst* Cu-only SOD was measured, and its biochemical features and subcellular localization were characterized. Furthermore, the function of *PsSOD2* was determined by transient expression in *N. benthamiana* and a BSMV-HIGS system in wheat-*Pst* interactions. The results suggest that *PsSOD2* works as a virulence factor and confers enhanced resistance to host-derived ROS during *Pst* infection.

Cu-only SODs represent a new class of SOD enzymes that are unique to fungi and oomycetes (Peterson *et al.*, 2016; Robinett *et al.*, 2017). In this study, bioinformatics analysis showed that each of five rust fungi with different hosts only contains an extracellular Cu-only SOD with the GPI anchor. Evolutionary conservation appears to imply importance of this kind of SODs for rust virulence. In addition, Cu-only SODs are exclusively extracellular and seem to be largely attached to the cell surface through GPI anchors (Schatzman *et al.*, 2020). In *C. albicans* cells, the two SODs SOD4 and SOD5 localize predominantly in the cell wall (Schatzman *et al.*, 2020). Unlike them, *PsSOD2* is shown to be specially localized to the plasma membrane. Previous studies have

also found that activity of the Cu-only SOD is inhibited at alkaline pH (Ellerby *et al.*, 1996). However, the optimum pH of PsSOD2 is approximately 10, similar to PsSOD1 (Liu *et al.*, 2016), which is possibly involved in the microenvironment at the wheat-*Pst* interface. Meanwhile, it is noteworthy that lower temperature optimum of PsSOD2 may be due to *Pst* requirement for cold. These results indicate that different Cu-only SODs show a great difference in biochemical characteristics, although they are conserved in Cu²⁺ binding sites.

Microorganisms need to sense and respond to constantly changing microenvironments, and adapt their transcriptome, proteome, and metabolism accordingly to survive (Brunke and Hube, 2014). Previous studies have found that the transcription of fungal SODs is induced by various stress challenges. For example, in *Schizosaccharomyces pombe*, the expression of *SOD1* was up-regulated by treatment with oxidants such as H₂O₂ and menadione (Lee *et al.*, 2002). *SOD5* transcripts were increased when *C. albicans* cells were subjected to osmotic or oxidative stresses (Martchenko *et al.*, 2004). In addition, Iron starvation led to increased expression of *sodA* of *Aspergillus nidulans* (Oberegger *et al.*, 2000) and *SOD4* of *C. albicans* (Schatzman *et al.*, 2020). In the present study, it is shown that *PsSOD2* expression was strongly up-regulated during *Pst* infection of wheat, whereas no expression difference was observed when urediniospores were germinated on distilled water. This result indicates that specific expression of *PsSOD2* is possibly due to certain inducers from host cells. Wang *et al.* (2007) reported that ROS were accumulated in *Pst*-infected wheat leaves, while the promoter of *PsSOD2* responded to ROS treatment. Therefore, it is a reasonable inference that the expression of *PsSOD2* was induced by host-derived ROS in wheat-*Pst* infections, which is possibly a coping scheme to guard *Pst* against host resistance. Many pathogens have been armed with additional SODs to function in the hostile climate of the host-pathogen interface (Broxton and Culotta, 2016). Cu-only SODs are found in many fungal pathogens where they combat the oxidative burst of the host and promote virulence. For example, *C. albicans* cell surface SODs (*SOD4* and *SOD5*) degrade extracellular ROS (produced during

host-pathogen interactions) to evade host immune surveillance in vivo (Frohner *et al.* 2009). SOD3 is required for *H. capsulatum* pathogenicity, allowing it to survive the oxidative burst of the host immune response (Youseff *et al.*, 2012). PbSOD3 has been proved to contribute to extracellular SOD activity of *Paracoccidioides spp.* And additively to antioxidation and virulence (Tamayo *et al.* 2016). In this study, heterologous transient assays of *PsSOD2* suppressed ROS accumulation. Conversely, H₂O₂ accumulation and enhanced resistance phenotypes were observed in HIGS wheat seedlings infected with *Pst*. Based on essential ROS scavenging mechanisms, H₂O₂ production mainly depends on SODs (dismutating superoxide anions into H₂O₂) and catalases (cleaving H₂O₂). Some reports have indicated that KatG2 catalases (with the SP) contribute to fungal virulence by degrading H₂O₂ produced during host-pathogen interactions (BeltránGarcía *et al.*, 2006; Zámocky *et al.*, 2009). For example, deletion of the KatG2 catalase from *Fusarium graminearum*, exclusively located on the cell wall of invading hyphal cells, reduced the virulence in wheat spike infection (Guo *et al.*, 2019). In addition, several secreted catalases, possibly participating in exogenous ROS removal, have been found in the *Pst* genome (Zheng *et al.*, 2013). There is no doubt that knockdown of *PsSOD2* resulted in superoxide anion accumulation. Previous studies have found that superoxide radicals inhibited enzymatic activity of catalase (Kono and Fridovich, 1982). Thus H₂O₂ was still accumulated and detected possibly due to inactivity of catalases, although silencing of *PsSOD2* led to decreased H₂O₂ production. In addition, histological observation showed that *Pst* growth was significantly blocked in HIGS plants, resulting in a reduction in the number of uredia. It is well known that the apoplastic oxidative burst may be sufficiently cytotoxic to kill pathogens as reported previously by Collins *et al.* (2003) and Wu *et al.* (1995). Meanwhile, ROS can also act as signaling molecules, triggering plant immune and cell death responses (Torres *et al.*, 2006). Therefore restricted fungal development and reduced disease symptoms are possibly due to increased ROS accumulation.

Recent work suggests that host derived Cu is used as an antipathogenic weapon; thus both host and pathogens actively engage cellular processes to manipulate Cu levels at key sites during pathogen infections (Fu *et al.*, 2014). For example, Cu can become very high in activated macrophages (White *et al.*, 2009). Likewise, Cu can also become high in specific host niches, such as in lungs infected with *C. neoformans* and in the bloodstream during *C. albicans* and *C. neoformans* invasion (Ding *et al.*, 2013; Li *et al.*, 2015). Conversely, the bacterial pathogen *Xanthomonas oryzae* overcomes rice defenses by transcriptionally activating the susceptibility gene *Xa13*, which cooperates with two Cu transporters, COPT1 and COPT5, to promote removal of copper from xylem vessels (Yuan *et al.*, 2010). In this study, some Cu efflux-involved genes were shown to be induced during *Pst* infection of wheat, whereas no significant change was observed for *COPTs* responsible for Cu uptake. This result appears to indicate that host responds to *Pst* infection by Cu efflux into the apoplast, which is unfavorable for pathogen invasion. In addition, activity of fungal SODs is limited by the availability of its Cu co-factor (Broxton and Culotta, 2016). In this study, PsSOD2 was shown to be Cu-dependent. To some extent, increased Cu concentration in the apoplast may activate PsSOD2, benefiting fungal infection. Interestingly, the functions of SODs on Cu resistance were also reported in *C. albicans* (Broxton and Culotta, 2016) and *S. cerevisiae* (Culotta *et al.*, 1995). Thus, it is a reasonable inference that presence of Cu-binding SODs is possibly an adaptive strategy evolved by pathogens to counteract Cu toxicity. The SODs on the surface of fungal pathogens are able to capture the host Cu, fueling these enzyme molecules to scavenge the superoxide anion produced during host-pathogen interactions (Fig. 9).

PsSOD2 was shown to confer enhanced *Pst* resistance to host-derived oxidative stress, which is similar to *PsSOD1* described previously by Liu *et al.* (2016). However, *PsSOD2* also exhibited obvious differences in some aspects compared with *PsSOD1*. For example, *PsSOD2* expression was up-regulated earlier (at 6 hpi) and continued for a longer time, indicating that *PsSOD2*

possibly functions earlier than *PsSOD1* during *Pst* infection. Subcellular localization analysis showed that PsSOD1 was secreted into the apoplast to scavenge exogenous ROS, while PsSOD2 was localized to the plasma membrane, seeming to provide more direct protection of *Pst* from host-derived oxidative stress. In addition, cofactor dependence differences indicate that *Pst* may adapt to host Cu variations by adjusting its metal co-factor selection for SODs. When host Cu is high, Cu-dependent SODs are employed, but when host Cu is low, *Pst* will switch to a non-Cu alternative. These differences suggest different types of fungal SODs are evolved and regulated to adapt complex microenvironment at the host-pathogen interface.

In conclusion, the present study revealed the key role of a Cu-only SOD (PsSOD2) during *Pst* infection. During wheat-*Pst* interactions, ROS induced PsSOD2, as a virulence factor, was localized to the plasma membrane and promoted *Pst* infection by guarding against superoxide toxicity derived from host (Fig. 9).

Experimental Procedures

Plant materials, pathogens and treatments

Wheat (*Triticum aestivum* L.) accession Su11 and the virulent *Pst* pathotype CYR32 were used in this study. Wheat inoculation with *Pst* were performed as described previously (Liu *et al.*, 2015). The suspension of *Pst* urediniospores was prepared with sterile water, these urediniospores were then transferred to the surface of wheat seedling leaves using a soft bristle brush. Nongerminated and germinated urediniospores were harvested and CYR32-infected wheat leaves were sampled at 6, 12, 18, 24, 36, 48, 72, 96, 120, 168, 216 and 264 hpi for expression profile analysis of *PsSOD2*. DNA and RNA extraction and cDNA synthesis were conducted in accordance with previous reports (Liu *et al.*, 2015). The expression patterns of *HMA*s and *COPT*s were analyzed based on an open-access exp-VIP platform (Borrill *et al.*, 2016). *N. benthamiana*, which was used for transient expression mediated by *Agrobacterium tumefaciens*, was grown at 25°C under a long photoperiod (16 h light:8 h darkness).

Characterization of SODs from five rust genomes

To obtain the SOD genes from five sequenced rust fungi *P. striiformis*, *P. graminis*, *P. triticina*, *P. sorghi* and *M. larici-populina*, all protein-coding genes from the five rust genomes were downloaded from the NCBI and analyzed as following workflow: all protein sequences were aligned to two intergrated protein sequence databases: SwissProt (Boeckmann *et al.*, 2003) and non-redundant (NR, NCBI) (Pruitt *et al.*, 2007) databases. Protein domains were annotated by searching against the InterPro (V32.0) (Hunter *et al.*, 2009) and Pfam (V27.0) (El-Gebali *et al.*, 2019) databases using InterProScan (Quevillon *et al.*, 2005) and HMMER (Johnson *et al.*, 2010), respectively.

The Gene Ontology (GO) terms for each gene were obtained from the corresponding InterPro or Pfam entry. The pathways in which the genes might be involved were assigned by BLAST against the KEGG databases, with an E-value cutoff of 1e-5. SOD annotation results were finally merged from the above two strategies.

The SP and GPI-anchor prediction of the SODs from different rust genomes was then performed on basis of SignalP 4.1 (<http://www.cbs.dtu.dk/services/SignalP/>) and PredGPI (<http://gpcr.biocomp.unibo.it/predgpi/pred.htm>).

Cloning of *PsSOD2* and sequence analysis

Transcriptome analysis of *Pst*-infected wheat leaves revealed that the *PsSOD2* gene was strongly induced (Hao *et al.*, 2016) during *Pst* infection. Thus, *PsSOD2* was amplified via RT-PCR using a CYR32-infected wheat cDNA sample as a template. The physicochemical characteristics of *PsSOD2* (GenBank accession number KNE95284) were investigated using the ProtParam tool at ExPASy (<https://web.expasy.org/protparam/>). The Pfam tool (<http://pfam.sanger.ac.uk/>) was then used to analyze the protein domain of *PsSOD2*. Finally, BLASTP analysis of *PsSOD2* against NR databases was conducted to obtain homologous proteins. Selected protein sequences along with *PsSOD2* were compared using ClustalW multiple sequence alignment software. MEGA 7.0 was then used to construct a phylogenetic tree based on the neighbour-joining method.

In addition, the coding sequences of *PsSOD2* among five sequenced *Pst* isolates, including a

Chinese CYR32 isolate, three US isolates (PST21, PST43 and PST08/21) and a UK isolate (PST87-7), were compared to identify gene polymorphisms. To obtain the corresponding nucleotide sequences, local BLAST searches were performed using BioEdit software (<http://www.mbio.ncsu.edu/BioEdit/bioedit.html>). DNAMAN software was then used to determine nucleotide substitutions in *PsSOD2*. Compared with CYR32, nucleotide substitutions of *PsSOD2* from different *Pst* isolates were counted and summed throughout all positions in the gene.

qRT-PCR analysis

The expression levels of *PsSOD2* were measured at different *Pst* infection stages by qRT-PCR as previously described by Liu *et al.* (2016). Elongation factor-1 (*PsEF1*) was used as the internal reference to normalize the gene expression in *Pst* (Yin *et al.*, 2009). Each reaction was performed in triplicate, and three non-template controls were contained in the experiment. The specificity of the amplicon was confirmed at the end of the PCR run using dissociation curve analysis. Two parameters, i.e., a relative quantity of RNA at least twofold higher or lower than the controls and $P < 0.005$, were used to assess the significance of the differences between time points. Similarly, the expression profiles of *HMA*s and *COPT*s in wheat-*Pst* interactions were assayed as mentioned above. The wheat elongation factor 1 (*TaEF1*) was employed as the endogenous reference (Liu *et al.*, 2015).

The primers used for qRT-PCR are listed in Supporting Information Table S3.

GUS activity assay

To analyze the responsiveness of the *PsSOD2* promoter to ROS, a 2,000-bp region upstream of *PsSOD2* was amplified by PCR using genomic DNA of *Pst* as a template. The promoter fragments were cloned into the *Xba*I/*Bam*HI restriction sites in plasmid pCB308 (Xiang *et al.*, 1999), generating the pCB308-*PsSOD2np* construct. The recombinant plasmid pCB308-*PsSOD2np* was transformed into GV3101 and infiltrated into *N. benthamiana* leaves. After 48 h, the infiltrated *N. benthamiana* leaves were sprayed with distilled water (control) or 10 mM H₂O₂ containing 0.025%

Tween 20, respectively, and then sampled at 1, 2 and 6 h post treatment (hpt). Total proteins extraction and quantitative GUS assays were performed as described previously by Huai *et al.* (2019). Fluorescence strength was measured on an Infinite 200 PRO Multimode Plate Reader (Tecan Life Sciences) with the excitation at 455 nm and emission at 365 nm. Three biological replicates were carried out to measure the GUS activity.

The primers used for plasmid constructions are listed in Supporting Information Table S3.

Expression and biological activity assay of PsSOD2 fusion proteins

For the biochemical characterization of PsSOD2, the ORF without the SP and GPI anchor sequence was amplified and inserted into the *EcoRI/XhoI* restriction sites of vector pET15b-sumo to generate the recombinant plasmid pET15b-sumo-*PsSOD2*. The *E. coli* Rossetta (DE3) competent cells were transformed with the recombinant pET15b-sumo-*PsSOD2* plasmid and then protein expression was induced by IPTG supplement overnight at 28°C. The collected cells were sonicated and the supernatant was examined by SDS-PAGE. The purified fusion protein was gained using a HisTrap FF affinity column (GE Healthcare, Uppsala, Sweden) and identified using Western blotting as described by Liu *et al.* (2016).

SOD activity assay was performed as previously described (Liu *et al.*, 2016). The thermal stabilities and pH optima of PsSOD2 were evaluated after the enzyme solutions were preincubated at 20-70°C and pH 5-13 for 30 min, respectively. The residual SOD activity of each treatment was then assayed. The influences of four metal ions (0.5 mM Cu²⁺, Zn²⁺, Mn²⁺ or Fe³⁺) on the enzymatic activity of the purified PsSOD2 were investigated. The residual activity was measured after enzyme solutions containing different metal ions were incubated in 50 mM phosphate buffer (pH 8.0) at 25°C for 30 min. Detection and removal of the metal ions in enzyme solutions were carried out as previously described (Liu *et al.*, 2016). All assays were repeated three times.

The primers used for plasmid constructions are listed in Supporting Information Table S3.

Functional identification of the SP of PsSOD2

The predicted SP of PsSOD2 was identified with a yeast secretion system (Jacobs *et al.*, 1997). The yeast signal sequence gene trap vector pSUC2 carrying a truncated invertase without initiation methionine and signal peptide, was used. DNA fragments encoding the predicted signal peptide of PsSOD2 (*PsSOD2_{sp}*), a effector protein from *Phytophthora sojae* Avr1b (*Avr1b_{sp}*, the positive control) and the first 25 amino acids of a non-secreted protein from *Magnaporthe oryzae* Mg87 (*Mg87₁₋₇₅*, the negative control) (Gu *et al.*, 2011) were inserted into the *EcoRI/XhoI* restriction sites of vector pSUC2, respectively. The yeast strain YTK12 was transformed with the recombinant plasmids pSUC2-*PsSOD2_{sp}*, pSUC2-*Avr1b_{sp}* and pSUC2-*Mg87₁₋₇₅*, and the empty vector pSUC2, respectively. To assess invertase secretion, positive transformants were inoculated on CMD-W medium (0.67% yeast nitrogen base without amino acids, 0.075% tryptophan dropout supplement, 2% sucrose, 0.1% glucose and 2% agar) and YPRAA medium (1% yeast extract, 2% peptone, 2% raffinose, 2 mg/ml antimycin A and 2% agar). The invertase enzymatic activity was also detected by the reduction of TTC to insoluble red colored 1, 3, 5-triphenylformazan (TPF) as described previously (Xu *et al.*, 2019).

The primers used for plasmid constructions are listed in Supporting Information Table S3.

Subcellular localization of PsSOD2 in *N. benthamiana*

To determine subcellular localization of PsSOD2, the coding sequence of GFP was inserted after the SP sequence (nucleotides 1–84) of *PsSOD2* using over-lap PCR (direct N-terminal or C-terminal fusion will result in GFP removal from PsSOD2, when the SP or the GPI anchor is cleaved). *PsSOD2_{sp}-GFP-PsSOD₈₅₋₅₇₆* was then recombined into pK7FWG2 (Karimi *et al.*, 2002) by Gateway technology. Similarly, pK7FWG2-*PsSOD2_{sp}-GFP-PsSOD₈₅₋₅₀₇* (without the GPI anchor sequence, nucleotides 508–576) was also constructed. The constructed recombinant plasmids were transformed into agrobacteria and infiltrated into *N. benthamiana* leaves. After two days, GFP and chlorophyll fluorescence signals were monitored by confocal microscope. Plasmolysis was performed by incubating the tobacco leaves in 1 M sorbitol for 30 min.

The primers used for plasmid constructions are listed in Supporting Information Table S3.

Measurement of oxidative burst

After agrobacteria containing the recombinant pK7FWG2-*PsSOD2*_{sp}:*GFP*: *PsSOD2*₈₅₋₅₇₆ plasmid were infiltrated into *N. benthamiana* leaves for two days, leaf disks were punched and floated on 200 µl water in a 96-well plate. 16 h after incubation, the water was removed and substituted with inducing buffer (100 nM flg22, 20 µg/ml peroxidase and 100 mM Luminol). Luminescence was detected over a period of 50 min using a TriStar2 microplate reader (Berthold Tech, Bad Wildbad, Germany). *N. benthamiana* leaves expressing GFP were used as the control. Western blotting using anti-GFP antibodies (Sigma-Aldrich) was performed to detect the expression of the GFP-*PsSOD2* fusion proteins in infiltrated leaves, following the protocol of Fu *et al.* (2014). Data presented were obtained from 36 leaf discs sampled from six independently infiltrated tobacco plants.

Barley stripe mosaic virus (BSMV)-mediated *PsSOD2* gene silencing in the compatible wheat-*Pst* interaction

The plasmids used for silencing *PsSOD2* were constructed as described in Holzberg *et al.* (2002). Two cDNA fragments derived from the coding region (161 bp, nucleotides 173–333) and (167 bp, nucleotides 332–498) were used to construct the recombinant plasmids *PsSOD2*-as1 and *PsSOD2*-as2, respectively, in an antisense orientation. *PsSOD2* was silenced using BSMV-HIGS as previously described by Liu *et al.* (2016). Two recombinant BSMV viruses (BSMV:*PsSOD2*-as1 and BSMV:*PsSOD2*-as2) were employed to inoculate wheat seedlings. After BSMV-inoculated wheat plants were incubated in a plant growth chamber for 9 days, the fourth leaves were further infected with CYR32, and sampled at 0, 24, 48 and 120 hpi for silencing efficiency calculations and histological observation (Wang *et al.*, 2007). BSMV:*TaPDS* and BSMV:γ act as controls for the BSMV infection. The 1 × FES buffer-inoculated wheat seedlings were used as the mock control. The disease phenotypes were observed and photographed at 15 dai. Fungal biomass was measured as previously described (Liu *et al.*, 2016).

Biological replicates were carried out in triplicate.

The primers used are listed in Supporting Information Table S3.

Histological observation of fungal growth and host response

To characterize the wheat-*Pst* interaction at the cytological level, the fungal development and host response were visualized microscopically. Fixation and staining of the leaf segments were carried out as described previously (Wang *et al.*, 2007). Difference of haustorial mother cells, haustoria, hyphal length and branches as well as colony size in the *PsSOD2*-silenced wheat plants was analyzed statistically compared with the control. In addition, H₂O₂ accumulation was observed at 24 and 48 hpi. No less than fifty infection sites from five randomly selected leaf segments were detected for each treatment.

Acknowledgements

This work was supported by the National Key Research and Development Program of China (grant no. 2016YFD0100602), Natural Science Basic Research Plan in Shaanxi Province of China (grant no. 2020JZ-12), National “111 plan” (grant no. BP0719026), Science Basic Research Plan in Shaanxi Province of China (grant no. 2019JCW-18) and National Undergraduate Training Programs for Innovation and Entrepreneurship (grant no. S201910712183).

Originality-Significance Statement

The authors confirm that the content of the manuscript is original, and the manuscript has neither been published previously, nor is being considered for publication elsewhere.

Conflict of interest

The authors declare no competing interests.

Reference

- Abba, S., Khouja, H.R., Martino, E., Archer, D.B., and Perotto, S. (2009) SOD1-targeted gene disruption in the ericoid mycorrhizal fungus *Oidiodendron maius* reduces conidiation and the capacity for mycorrhization. *Mol Plant Microbe Interact* **22**: 1412–1421.
- Apel, K., and Hirt, H. (2004) Reactive oxygen species: metabolism, oxidative stress, and signal

transduction. *Annu Rev Plant Biol* **55**: 373–399.

- Bafana, A., Dutt, S., Kumar, S., and Ahuja, P.S. (2010) Superoxide dismutase: an industrial perspective. *Crit Rev Biotechnol* **31**: 65–76.
- Baxter, A., Mittler, R., and Suzuki, N. (2014) ROS as key players in plant stress signalling. *J Exp Bot* **65**: 1229–1240.
- BeltránGarcía, M.J., OguraFujii, T., ManzoSánchez, G., and Arias-Castro, C. (2006) Catalases of phytopathogenic fungi: factors of virulence and resistance to fungicides? *Rev Mex Fitopatol* **24**: 50–58.
- Blokhina, O., Virolainen, E., Fagerstedt, K.V. (2003) Antioxidants, oxidative damage and oxygen deprivation stress: a review. *Ann Bot* **91**: 179–194.
- Boeckmann, B., Bairoch, A., Apweiler, R., Blatter, M., Estreicher, A., Gasteiger, E., *et al.* (2003) The SWISS-PROT protein knowledgebase and its supplement TrEMBL in 2003. *Nucleic Acids Res* **31**: 365-370.
- Borrill, P., Ramirez-Gonzalez, R., and Uauy, C. (2016) expVIP: A customizable RNA-seq data analysis and visualization platform. *Plant Physiol* **170**: 2172–2186.
- Briones-Martin-del-Campo, M., Orta-Zavalza, E., Cañas-Villamar, I., Gutiérrez-Escobedo, G., Juárez-Cepeda, J., Robledo-Márquez, K., *et al.* (2015) The superoxide dismutases of *Candida glabrata* protect against oxidative damage and are required for lysine biosynthesis, DNA integrity and chronological life survival. *Microbiology* **161**: 300–310.
- Broxton, C.N., and Culotta, V.C. (2016) SOD enzymes and microbial pathogens: surviving the oxidative storm of infection. *PLoS Pathog* **12**: e1005295.
- Brunke, S., and Hube, B. (2014) Adaptive Prediction as a Strategy in Microbial Infections. *PLoS Pathog* **10**: e1004356.
- Collins, N.C., Thordal-Christensen, H., Lipka, V., Bau, S., Kombrink, E., Qiu, J.L., *et al.* (2003) SNARE-protein-mediated disease resistance at the plant cell wall. *Nature* **425**: 973–977.
- Culotta, V.C., Joh, H.D., Lin, S.J., Slekar, K.H., and Strain, J. (1995) Physiological Role for

Saccharomyces cerevisiae Copper/Zinc Superoxide Dismutase in Copper Buffering. *J Biol Chem* **270**: 29991–29997.

Ding, C., Festa, R.A., Chen, Y.L., Espart, A., Palacios, O., Espin, J., *et al.* (2013) *Cryptococcus neoformans* copper detoxification machinery is critical for fungal virulence. *Cell Host Microbe* **13**: 265–276.

Eitinge, T. (2004) In vivo production of active nickel superoxide dismutase from *Prochlorococcus marinus* MIT9313 is dependent on its cognate peptidase. *J Bacteriol* **186**: 7821–7825.

El-Gebali, S., Mistry, J., Bateman, A., Eddy, S.R., Luciani, A., Potter, S.C., *et al.* (2019) The Pfam protein families database in 2019. *Nucleic Acids Res* **47**: D427–D432.

Ellerby, L.M., Cabelli, D.E., Graden, J.A., and Valentine, J.S. (1996) Copper-zinc superoxide dismutase: Why not pH-dependent? *J Am Chem Soc* **118**: 6556–6561.

Fridovich, I. (1995) Superoxide radical and superoxide dismutases. *Annu Rev Biochem* **64**: 97–112.

Frohner, I.E., Bourgeois, C., Yatsyk, K., Majer, O., and Kuchler, K. (2009) *Candida albicans* cell surface superoxide dismutases degrade host-derived reactive oxygen species to escape innate immune surveillance. *Mol Microbiol* **71**: 240–52.

Fu, Y., Chang, F.M.J., and Giedroc, D.P. (2014) Copper transport and trafficking at the host-bacterial pathogen interface. *Acc Chem Res* **47**: 3605–3613.

Gleason, J.E., Galalaldeen, A., Peterson, R.L., Taylor, A.B., Holloway, S.P., Waninger-Saroni, J., *et al.* (2014) *Candida albicans* SOD5 represents the prototype of an unprecedented class of Cu-only superoxide dismutases required for pathogen defense. *Proc Natl Acad Sci USA* **111**: 5866–5871.

Gu, B., Kale, S.D., Wang, Q.H., Wang, D.H., Pan, Q.N., Cao, H., *et al.* (2011) Rust secreted protein Ps87 is conserved in diverse fungal pathogens and contains a RXLR-like motif sufficient for translocation into plant cells. *PLoS One* **6**: e27217.

Guo, Y., Yao, S., Yuan, T., Wang, Y.Z., Zhang, D., and Tang, W.H. (2019) The spatiotemporal

control of KatG2 catalase-peroxidase contributes to the invasiveness of *Fusarium graminearum* in host plants. *Mol Plant Pathol* **20**: 685–700.

Hao, Y.B., Wang, T., Wang, K., Wang, X.J., Fu, Y.P., Huang, L.L., Kang, Z.S. (2016)

Transcriptome analysis provides insights into the mechanisms underlying wheat plant resistance to stripe rust at the adult plant stage. *PLoS One* **11**: e0150717.

Holzberg, S., Brosio, P., Gross, C., and Pogue, G.P. (2002) Barley stripe mosaic virus induced gene silencing in a monocot plant. *Plant J* **30**: 315–327.

Huai, B.Y., Yang, Q., Qian, Y.R., Qian, W.H., Kang, Z.S., and Liu, J. (2019) ABA-induced sugar transporter TaSTP6 promotes wheat susceptibility to stripe rust. *Plant Physiol* **181**: 1328–1343.

Hunter, S., Apweiler, R., Attwood, T.K., Bairoch, A., Bateman, A., Binns, D., *et al.* (2009)

InterPro: the integrative protein signature database. *Nucleic Acids Res* **37**: D211–D215.

Hwang, C.S., Rhie, G.E., Oh, J.H., Huh, W.K., Yim, H.S., and Kang, S.O. (2002) Copper- and zinc-containing superoxide dismutase (Cu/ZnSOD) is required for the protection of *Candida albicans* against oxidative stresses and the expression of its full virulence. *Microbiology* **148**: 3705–3713.

Jackson, T.A., and Brunold, T.C. (2004) Combined spectroscopic/computational studies on Fe- and Mn-dependent superoxide dismutases: insights into second-sphere tuning of active site properties. *Acc Chem Res* **37**: 461–470.

Jacobs, K.A., Collins-Racie, L.A., Colbert, M., Duckett, M., Golden-Fleet, M., Kelleher, K., *et al.*

(1997) A genetic selection for isolating cDNAs encoding secreted proteins. *Gene* **198**: 289–296.

Johnson, L.S., Eddy, S.R., Portugaly, E. (2010) Hidden Markov model speed heuristic and iterative HMM search procedure. *BMC Bioinformatics* **11**: 431.

Kadota, Y., Shirasu, K., and Zipfel, C. (2015) Regulation of the NADPH Oxidase RBOHD during plant immunity. *Plant Cell Physiol* **56**: 1472–1480.

Kadota, Y., Sklenar, J., Derbyshire, P., Stransfeld, L., Asai, S., Ntoukakis, V., *et al.* (2014) Direct Regulation of the NADPH Oxidase RBOHD by the PRR-associated kinase BIK1 during plant

immunity. *Mol Cell* **54**: 43–55.

Karimi, M., Inze, D., and Depicker, A. (2002) GATEWAY vectors for agrobacterium-mediated plant transformation. *Trends Plant Sci* **7**: 193–195.

Kono, Y., and Fridovich, I. (1982) Superoxide radical inhibits catalase. *J Biol Chem* **257**: 5751.

Lambou, K., Lamarre, C., Beau, R., Dufour, N., and Latge, J.P. (2010) Functional analysis of the superoxide dismutase family in *Aspergillus fumigatus*. *Mol Microbiol* **75**: 910–923.

Lee, J., Kwon, E.S., Kim, D.W., Cha, J., and Roe, J.H. (2002) Regulation and the role of Cu, Zn-containing superoxide dismutase in cell cycle progression of *Schizosaccharomyces pombe*. *Biochem Biophys Res Commun* **297**: 854–862.

Li, C.X., Gleason, J.E., Zhang, S.X., Bruno, V.M., Cormack, B.P., and Culotta, V.C. (2015) *Candida albicans* adapts to host copper during infection by swapping metal cofactors for superoxide dismutase. *Proc Natl Acad Sci USA* **112**: E5336–E5342.

Liu, J., Guan, T., Zheng, P.J., Chen, L.Y., Yang, Y., Huai, B.Y., *et al.* (2016) An extracellular Zn-only superoxide dismutase from *Puccinia striiformis* confers enhanced resistance to host-derived oxidative stress. *Environ Microbiol* **18**: 4118–4135.

Liu, J., Han, L.N., Huai, B.Y., Zheng, P.J., Chang, Q., Guan, T., *et al.* (2015) Down-regulation of a wheat alkaline/neutral invertase correlates with reduced host susceptibility to wheat stripe rust caused by *Puccinia striiformis*. *J Exp Bot* **66**: 7325–7338.

Lu, X., Wang, C., and Liu, B. (2015) The role of Cu/Zn-SOD and Mn-SOD in the immune response to oxidative stress and pathogen challenge in the clam *Meretrix meretrix*. *Fish Shellfish Immunol* **42**: 58–65.

Martchenko, M., Alarco, A.M., Harcus, D., and Whiteway, M. (2004) Superoxide dismutases in *Candida albicans*: transcriptional regulation and functional characterization of the hyphal-induced SOD5 gene. *Mol Biol Cell* **15**: 456–467.

Mccord, J.M., and Fridovich, I. (1969) Superoxide dismutase. An enzymic function for

erythrocuprein (hemocuprein). *J Biol Chem* **244**: 6049–6055.

Miller, A.F. (2012) Superoxide dismutases: ancient enzymes and new insights. *FEBS Lett* **586**: 585–595.

Mittler, R., Vanderauwera, S., Gollery, M., and Van Breusegem, F. (2004) Reactive oxygen gene network of plants. *Trends Plant Sci* **9**: 490–498.

Morrissey, J. and Bowler, C. (2012) Iron utilization in marine cyanobacteria and eukaryotic algae. *Front Microbiol* **3**: 43.

Narasipura, S.D., Chaturvedi, V., and Chaturvedi, S. (2005) Characterization of *Cryptococcus neoformans* variety gattii SOD2 reveals distinct roles of the two superoxide dismutases in fungal biology and virulence. *Mol Microbiol* **55**: 1782–1800.

Oberegger, H., Zadra, I., Schoeser, M., and Haas, H. (2000) Iron starvation leads to increased expression of Cu/Zn-superoxide dismutase in *Aspergillus*. *FEBS Lett* **485**: 113–116.

O'Brien, K.M., Dirmeier, R., Engle, M., and Poyton, R.O. (2004) Mitochondrial protein oxidation in yeast mutants lacking manganese-(MnSOD) or copper- and zinc containing superoxide dismutase (CuZn-SOD): evidence that MnSOD and CuZnSOD have both unique and overlapping functions in protecting mitochondrial proteins from oxidative damage. *J Biol Chem* **279**: 51817–51827.

Peterson, R.L., Galaledeen, A., Villarreal, J., Taylor, A.B., Cabelli, D.E., Hart, P.J., *et al.* (2016) The phylogeny and active site design of eukaryotic copper-only superoxide dismutases. *J Biol Chem* **291**: 20911–20923.

Pilon, M., Ravet, K., Tapken, W. (2011) The biogenesis and physiological function of chloroplast superoxide dismutases. *Biochim Biophys Acta* **1807**: 989–998.

Pruitt, K.D., Tatusova, T., Maglott, D.R. (2007) NCBI reference sequences (RefSeq): a curated non-redundant 564 sequence database of genomes, transcripts and proteins. *Nucleic Acids Res* **35**: D61-D65.

Quevillon, E., Silventoinen, V., Pillai, S., Harte, N., Mulder, N., Apweiler, R., *et al.* (2005)

InterProScan: protein domains identifier. *Nucleic Acids Res* **33**: W116-W120.

- Robinett, N.G., Peterson, R.L., and Culotta, V.C. (2017) Eukaryotic Cu-only superoxide dismutases (SODs): A new class of SOD enzymes and SOD-like protein domains. *J Biol Chem* **293**: 4636–4643.
- Schatzman, S.S., Peterson, R.L., Teka, M., He, B., and Culotta, V.C. (2020) Copper-only superoxide dismutase enzymes and iron starvation stress in *Candida* fungal pathogens. *J Biol Chem* **295**: 570–583.
- Schmidt, A., Gube, M., Schmidt, A., and Kothe, E. (2009) In silico analysis of nickel containing superoxide dismutase evolution and regulation. *J Basic Microbiol* **49**: 109–118.
- Staerck, C., Gastebois, A., Vandeputte, P., Calenda, A., Larcher, G., Gillmann, L., *et al.* (2017) Microbial antioxidant defense enzymes. *Microb Pathog* **110**: 56–65.
- Tamayo, D., Munoz, J.F., Lopez, A., Uran, M., Herrera, J., Borges, C.L., *et al.* (2016) Identification and analysis of the role of superoxide dismutases isoforms in the pathogenesis of *Paracoccidioides spp.* *PLoS Negl Trop Dis* **10**: e0004481.
- Torres, M.A., Jones, J.D., and Dangl, J.L. (2006) Reactive oxygen species signalling in response to pathogens. *Plant Physiol* **141**: 373–378.
- Wang, C.F., Huang, L.L., Buchenauer, H., Han, Q.M., Zhang, H.C., and Kang, Z.S. (2007) Histochemical studies on the accumulation of reactive oxygen species ($O_2^{\bullet-}$ and H_2O_2) in the incompatible and compatible interaction of wheat-*Puccinia striiformis* f. sp. *tritici*. *Physiol Mol Plant Pathol* **71**: 230–239.
- White, C., Lee, J., Kambe, T., Fritsche, K., and Petris, M.J. (2009) A role for the ATP7A copper-transporting ATPase in macrophage bactericidal activity. *J Biol Chem* **284**: 33949–33956.
- Wu, G.S., Short, B.J., Lawrence, E.B., Levine, E.B., Fitzsimmons, K.C., and Shah, D.M. (1995) Disease resistance conferred by expression of a gene encoding H_2O_2 -generating glucose oxidase in transgenic potato plants. *Plant Cell* **7**: 1357–1368.

- Xiang, C., Han, P., Lutziger, I., Wang, K., and Oliver, D.J. (1999) A mini binary vector series for plant transformation. *Plant Mol Biol* **40**: 711–717.
- Xie, X.Q., Li, F., Ying, S.H., and Feng, M.G. (2012) Additive contributions of two manganese-cored superoxide dismutases (MnSODs) to antioxidation, UV tolerance and virulence of *Beauveria bassiana*. *PLoS One* **7**: e30298.
- Xu, Q., Tang, C.L., Wang, X.D., Sun, S.T., Zhao, J.R., Kang, Z.S., *et al.* (2019) An effector protein of the wheat stripe rust fungus targets chloroplasts and suppresses chloroplast function. *Nat Commun* **10**: 5571.
- Yoshida, Y., Maeda, T., Lee, B., and Hasunuma, K. (2008) Conidiation rhythm and light entrainment in superoxide dismutase mutant in *Neurospora crassa*. *Mol Genet Genomics* **279**: 193–202.
- Youn, H.D., Kim, E.J., Roe, J.H., Hah, Y.C., and Kang, S.O. (1996) A novel nickel-containing superoxide dismutase from *Streptomyces spp.* *Biochem J* **318**: 889–896.
- Youseff, B.H., Holbrook, E.D., Smolnycki, K.A., and Rappleye, C.A. (2012) Extracellular superoxide dismutase protects histoplasma yeast cells from host-derived oxidative stress. *PLoS Pathog* **8**: e1002713.
- Yuan, M., Chu, Z.H., Li, X.H., Xu, C.G., and Wang, S.P. (2010) The bacterial pathogen *Xanthomonas oryzae* overcomes rice defenses by regulating host copper redistribution. *Plant Cell* **22**: 3164–3176.
- Zámocky, M., Furtmüller, P.G., and Obinger, C. (2009) Two distinct groups of fungal catalase/oxidases. *Biochem Soc Trans* **37**: 772–777.
- Zeinali, F., Homaei, A., and Kamrani, E. (2015) Sources of marine superoxide dismutases: Characteristics and applications. *Int J Biol Macromol* **79**: 627–637.
- Zelko, I.N., Mariani, T.J., and Folz, R.J. (2002) Superoxide dismutase multigene family: a comparison of the CuZn-SOD (SOD1), Mn-SOD (SOD2), and EC-SOD (SOD3) gene structures, evolution and expression. *Free Radic Biol Med* **33**: 337–349.

Zheng, W.M., Huang, L.L., Huang, J.Q., Wang, X.J., Chen, X.M., Zhao, J., *et al.* (2013) High genome heterozygosity and endemic genetic recombination in the wheat stripe rust fungus
Nat Commun **4**: 2673.

Figure legends

Fig. 1 Expression of *PsSOD2* during *Pst* infection and exogenous H₂O₂ treatment. The means and error bars were calculated from three replicates. Bars indicate the standard deviation of the mean. Single ($P < 0.05$) and double asterisks ($P < 0.01$) indicate a significant difference from the control according to Student's *t* test. (A) The transcript levels of *PsSOD2* were calculated by the comparative Ct method with *PstEF1* as an internal standard. Relative quantifications are compared with the expression levels of nongerminated urediniospores. (B) *PsSOD2* promoter activity was induced by H₂O₂. *N. benthamiana* leaves infiltrated by GV3101 with

pCB308-*PsSOD2np* for 48 h were sprayed with a solution containing 10 mM of H₂O₂ and 0.025% (v/v) TWEEN 20 or with 0.025% (v/v) TWEEN 20 alone, and sampled at 0, 1, 2, and 6 hpt for GUS-activity. US, urediniospores; GT, germ tubes; MU, 4-methylumbelliferone.

Fig. 2. Biochemical characterization of PsSOD2. (A) The SDS-PAGE profiles of PsSOD2 expressed in *E. coli* BL21(DE3)plysS. Lane 1, uninduced *E. coli* cell lysates containing pET15b-sumo-*PsSOD2*; lane 2, *E. coli* cell lysates harbouring pET15b-sumo-*PsSOD2* induced by IPTG; lane 3, soluble fractions from the cell culture expressing *PsSOD2*; lane 4, insoluble fractions from the cell culture expressing *PsSOD2*; M, marker. (B) and (C) Thermal and pH stability of the purified PsSOD2. (D) Effects of metal ions on the activity of the purified PsSOD2. Asterisks indicate a significant difference ($P < 0.05$) compared with the control using Student's *t*-test.

Fig. 3. Functional characterization of the signal peptide of PsSOD2. (A) The PsSOD2 or Avr1b signal peptides or the first 25 amino acids of Mg87 were fused in-frame to the invertase sequence in the pSUC2 vector and transformed into the yeast YTK12 strain. Empty YTK12 strain and YTK12 containing pSUC2 were used as negative controls. Invertase secretion-deficient strains can grow on CMD-W medium but not on YPRAA medium. (B) The enzymatic activity of invertase was determined by the reduction of 2, 3, 5-Triphenyltetrazolium Chloride (TTC) to insoluble red colored 1, 3, 5-Triphenylformazan (TPF). The culture supernatants of the transformed cells were collected in tubes to assay the enzymatic activity of secreted invertase.

Fig. 4. Subcellular localization of PsSOD2. (A) Schematic representation of GFP-PsSOD2 and GFP-PsSOD2_{ΔGPI} fusion constructs. (B) GFP-PsSOD2 fusion proteins expressed in *N. benthamiana* leaves by *Agrobacterium*-mediated transient assays. (C) Subcellular localization of GFP-PsSOD2_{ΔGPI}. *Agrobacterium* infiltrated *N. benthamiana* leaves were incubated in 1 M sorbitol for 30 min. Cytoplasm shrinkage was easily observed in the leaf epidermal cells. Comparable expression and localization patterns were observed in two independent biological

replicates. Asterisks indicate cell wall and arrows indicate PsSOD2 secreted into the apoplast.

Bars =10 μm .

Fig. 5 PsSOD2 suppression of ROS in *N. benthamiana*. (A) ROS burst induced by 100 nM flg22 in discs of *N. benthamiana* leaves agro-infiltrated to express either GFP or GFP-PsSOD2. The rates of ROS production were measured in relative light units (RLU). (B) Western blotting analysis of GFP-PsSOD2 expression in *N. benthamiana* leaves using anti-GFP.

Fig. 6 *Pst* virulence was reduced in the *PsSOD2*-silenced wheat plants. (A) Mild chlorotic mosaic symptoms were observed on the fourth leaves of seedlings at 9 dai with BSMV, and bleaching was evident on the fourth leaves of plants inoculated by BSMV:*TaPDS*. Mock, wheat leaves infected with FES buffer. (B) Disease phenotypes of the fourth leaves pre-inoculated with BSMV and then challenged with CYR32. (C) Fungal biomass measurements using real-time PCR analysis of total DNA extracted from the wheat leaves infected by CYR32 at 15 dai. Ratio of total fungal DNA to total wheat DNA was assessed using the wheat gene *TaEF-1a* and the *Pst* gene *PstEF1*. (D) Silencing efficiency assay of *PsSOD2* in *Pst*. Wheat leaves inoculated with BSMV: γ and sampled after inoculation with CYR32 were used as the controls. The data were normalized to the expression level of *TaEF-1a*. The mean \pm SD from three independent samples is presented. Asterisks indicate a significant difference ($P < 0.05$) using Student's *t*-test.

Fig. 7 Histological observation of fungal growth and host response in BSMV: γ and recombinant BSMV inoculated wheat leaves infected with CYR32. (A-E) Fungal growth at 24 hpi (A) or 48 hpi (B), infection unit area at 120 hpi (C), H_2O_2 accumulation at 24 hpi (D) or 48 hpi (E) in BSMV: γ infected plants. (F-J) Fungal growth at 24 hpi (F) or 48 hpi (G), infection unit area at 120 hpi (H), H_2O_2 accumulation at 24 hpi (I) or 48 hpi (J) in BSMV:*PsSOD2*-infected plants, H_2O_2 accumulation was calculated using DAB staining. (K) The average number of HB, HMC and H showed no significant difference in HIGS plants infected by CYR32 compared with the control at 24 hpi. (L) Hyphal length, which is the average distance from the junction of the substomatal

vesicle and the hypha to the tip of the hypha, was clearly decreased in HIGS plants infected by CYR32 at 24 hpi. (M) The infection unit area at 120 hpi per infection unit was significantly reduced in HIGS plants infected by CYR32. (N) A significant increase in ROS accumulation was observed in CYR32-infected HIGS plants at 24 hpi. Values represent the means \pm SD of three independent samples. Differences were assessed using Student's *t*-tests. Asterisks indicate $P < 0.05$. SV, substomatal vesicle; HMC, haustorial mother cell; IH, infection hypha; HB, hyphal branch; H, haustoria.

Fig. 8 Expression profiles of wheat TaHMA genes during *Pst* infection. (A) Expression of *TaHMAs* is shown as a heatmap at 24, 48 and 72 hpi. Data are exhibited as $\log_2(\text{transcripts per million})$ ($\log_2\text{tpm}$). (B-D) Transcript levels of TraesCS7B02G320100, TraesCS2A02G162900 and TraesCS7D02G467100 are increased during *Pst* infection. Wheat leaves infected with CYR32 were collected at 0, 12, 24, 48, 72, and 120 hpi. Expression levels were normalized to *TaEF-1a*. Asterisks ($P < 0.05$) indicate a significant difference from the untreated control according to Student's *t* test. Bars indicate the mean \pm SD of three independent replicates.

Fig. 9 Possible model depicting the role of *PsSOD2* in the wheat-*Pst* interaction.

During *Pst* infection of wheat, ROS accumulation and Cu concentration is increased at the wheat-*Pst* interface. Increased ROS production can induce up-regulation of *PsSOD2*. Plasma membrane-localized *PsSOD2* binding Cu^{2+} counteracts host-derived oxidative stress and reduces Cu toxicity, promoting fungal infection.

Supporting Information

Fig. S1 Sequence characterization of PsSOD2. (A) Prediction of conserved domains of PsSOD2 from *Pst*. (B) Alignment of PsSOD2 against SOD4 (GenBank accession number AOW27120), SOD5 (GenBank accession number AOW27119) and SOD6 (GenBank accession number AOW27078) from *C. albican*. Copper ligands, blue; zinc ligands, green; disulfide Cys, purple; active site Arg, cyan; Δ EL, missing electrostatic loop.

Fig. S2 Prediction of the signal peptide and GPI anchor of PsSOD2. The signal peptide (A) and GPI anchor (B) of PsSOD2 were predicted using SignalP 4.1 (<http://www.cbs.dtu.dk/services/SignalP/>) and PredGPI (<http://gpcr.biocomp.unibo.it/predgpi/pred.htm>), respectively.

Fig. S3 Phylogenetic analysis of PsSOD2 and selected homologous proteins from other fungi. The unrooted phylogram was constructed based on the NJ method. The confidence level for the groupings was estimated using 1000 bootstrap replicates. The numbers adjacent to the branch points indicate the percentage of replicates supporting each branch.

Fig. S4 Multiple sequence alignment of PsSOD2 from different *Pst* isolates. Identical (*) and highly similar (:) amino acids are indicated. Red box: different amino acid substitutions; ▼ : Cu²⁺ binding site; blue line: conserved domain.

Fig. S5 (A) The SDS-PAGE profiles of the purified PsSOD2 proteins at different dilutions. (B) Western blotting analysis of the purified PsSOD2 proteins using anti-His. (C) Cu²⁺ ions dependence of PsSOD2. Single ($P < 0.05$) and double asterisks ($P < 0.01$) indicate a significant difference compared with the control using Student's *t*-test.

Fig. S6 HIGS of *PsSOD2* led to restricted fungal development and increased ROS accumulation in

the host cells. (A) The average number of HB, HMC and H showed no significant difference in HIGS plants infected by CYR32 compared with the control at 48 hpi. (B) Hyphal length was clearly decreased in HIGS plants infected by CYR32 at 48 hpi. (C) The infection unit area at 24 and 48 hpi per infection unit in HIGS plants infected by CYR32, was similar to that of the control. (D) A significant increase in ROS accumulation was observed in CYR32-infected HIGS plants at 48 hpi. Values represent the means \pm SD of three independent samples. Differences were assessed using Student's *t*-tests. Asterisks indicate $P < 0.05$. HMC, haustorial mother cell; IH, infection hypha; HB, hyphal branch; H, haustoria.

Fig. S7 Expression profiles of wheat TaCOPT genes during *Pst* infection. Expression of *TaCOPTs* is shown as a heatmap at 24, 48 and 72 hpi. Data are exhibited as $\log_2(\text{transcripts permillion})$ ($\log_2\text{tpm}$).

Table S1 The number of SODs containing the SP and GPI anchor in five *Puccinia* genuses.

Table S2 Overview of intraspecies nucleotide polymorphism in *PsSOD2*.

Table S3 Oligonucleotides and strains in this study.

Fig. 1

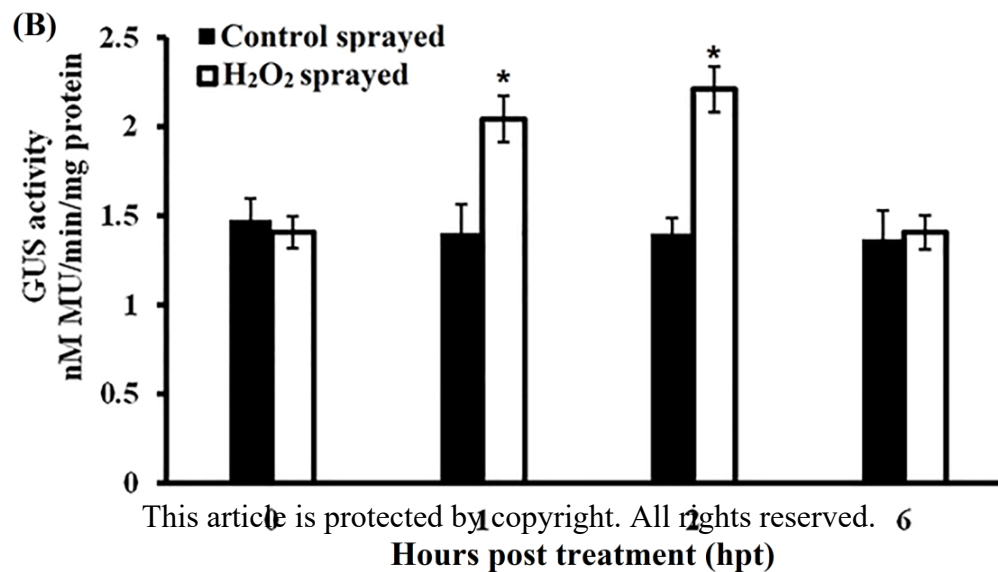
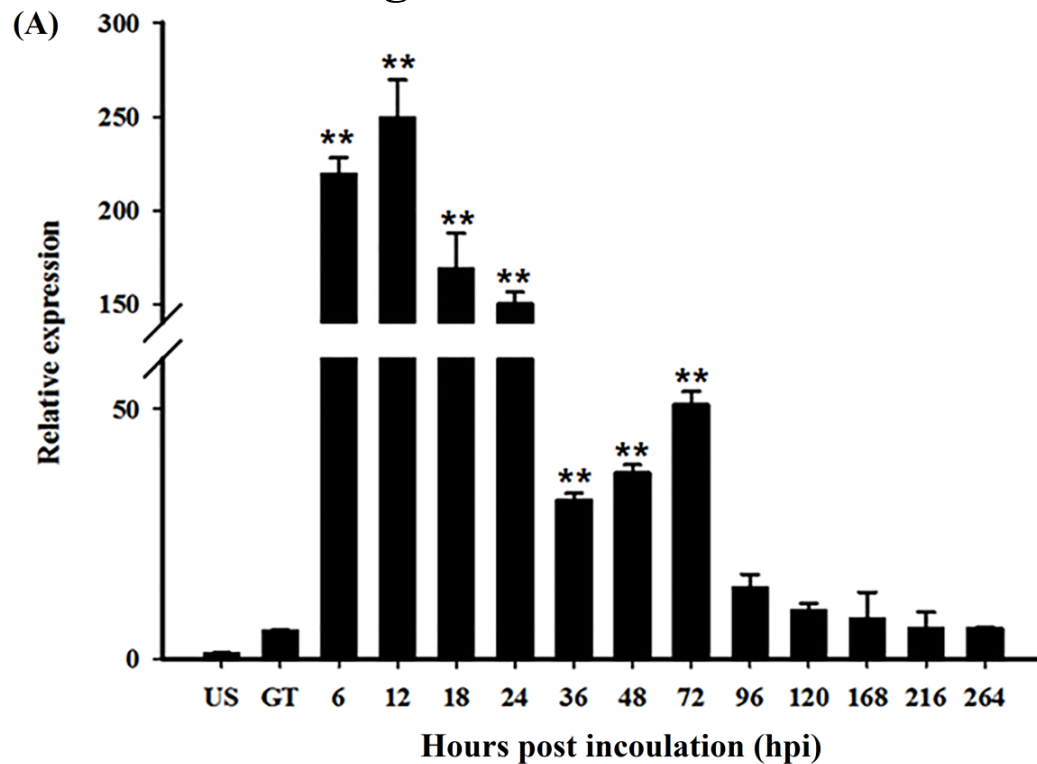


Fig. 2

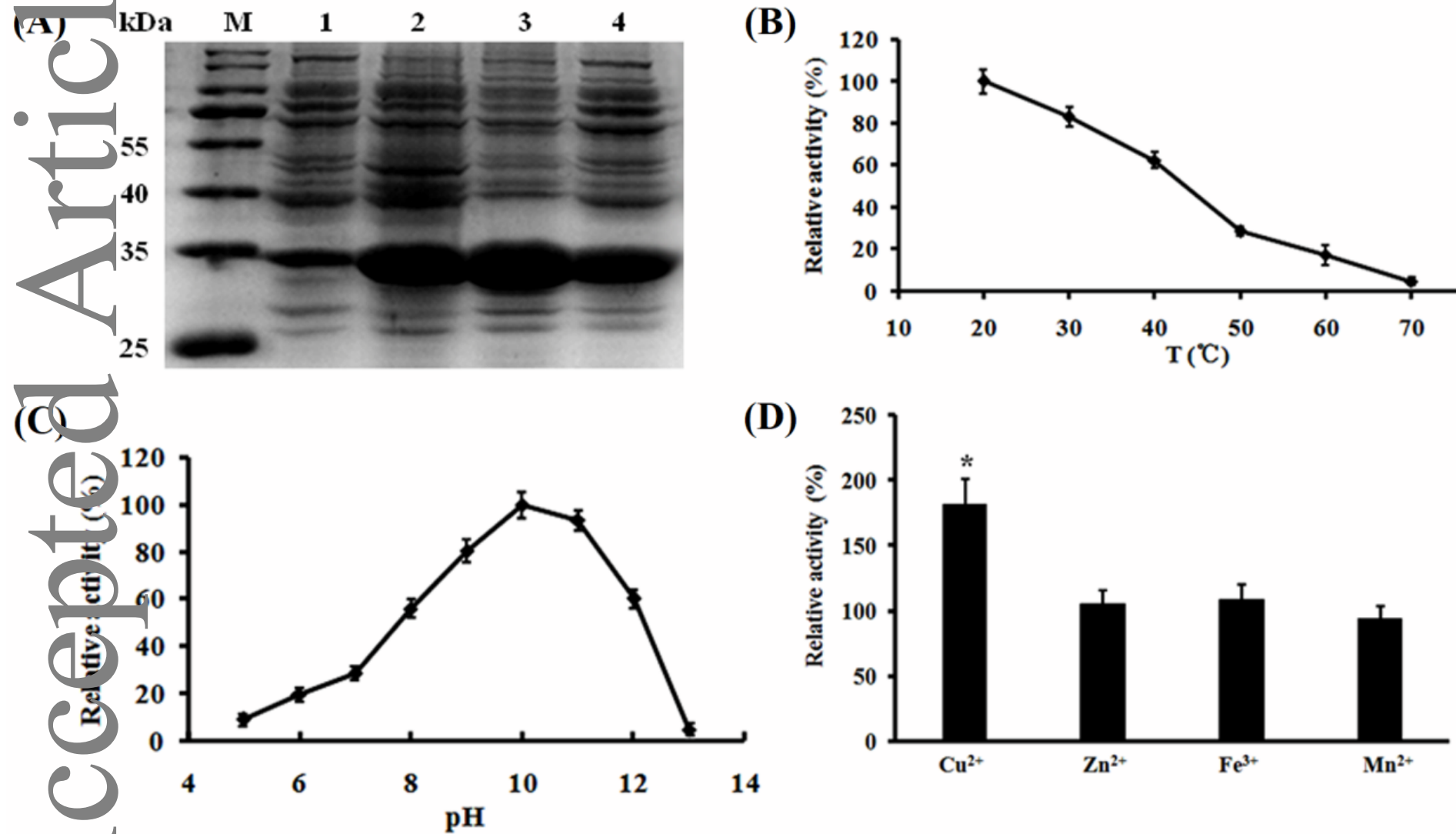


Fig. 3

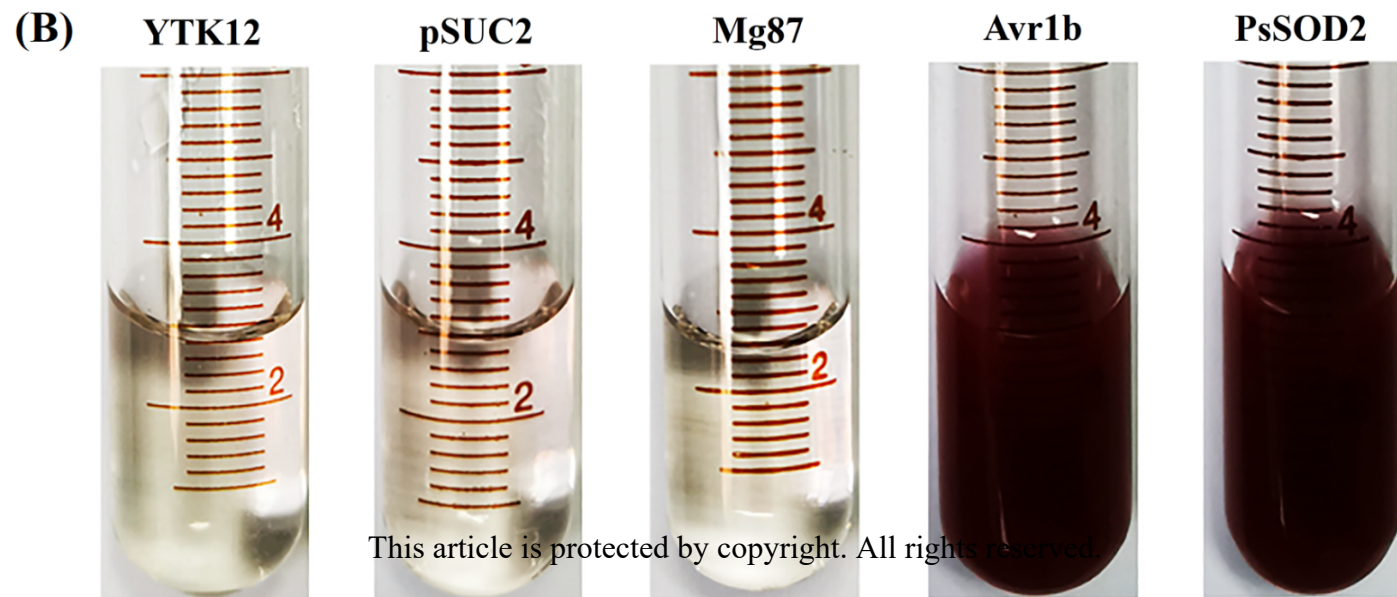
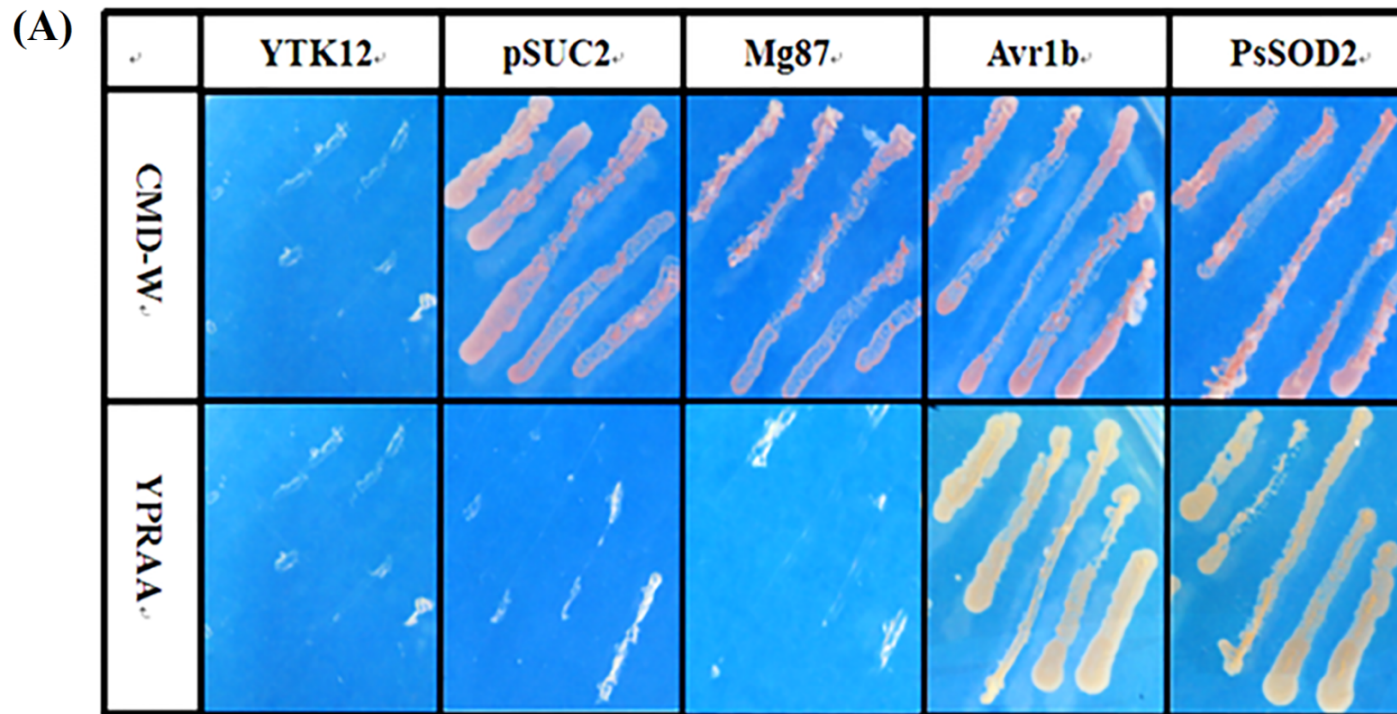


Fig. 4

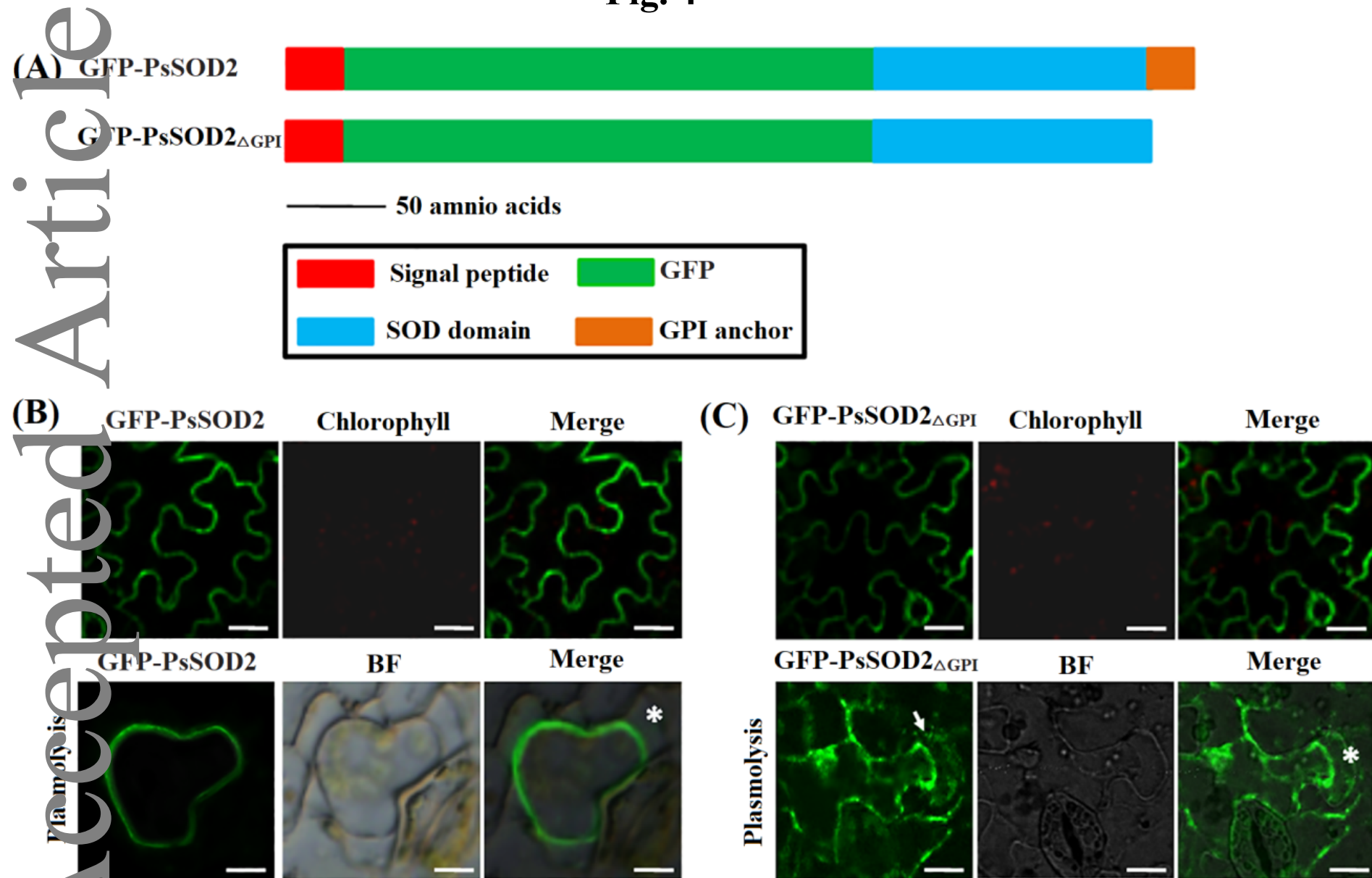
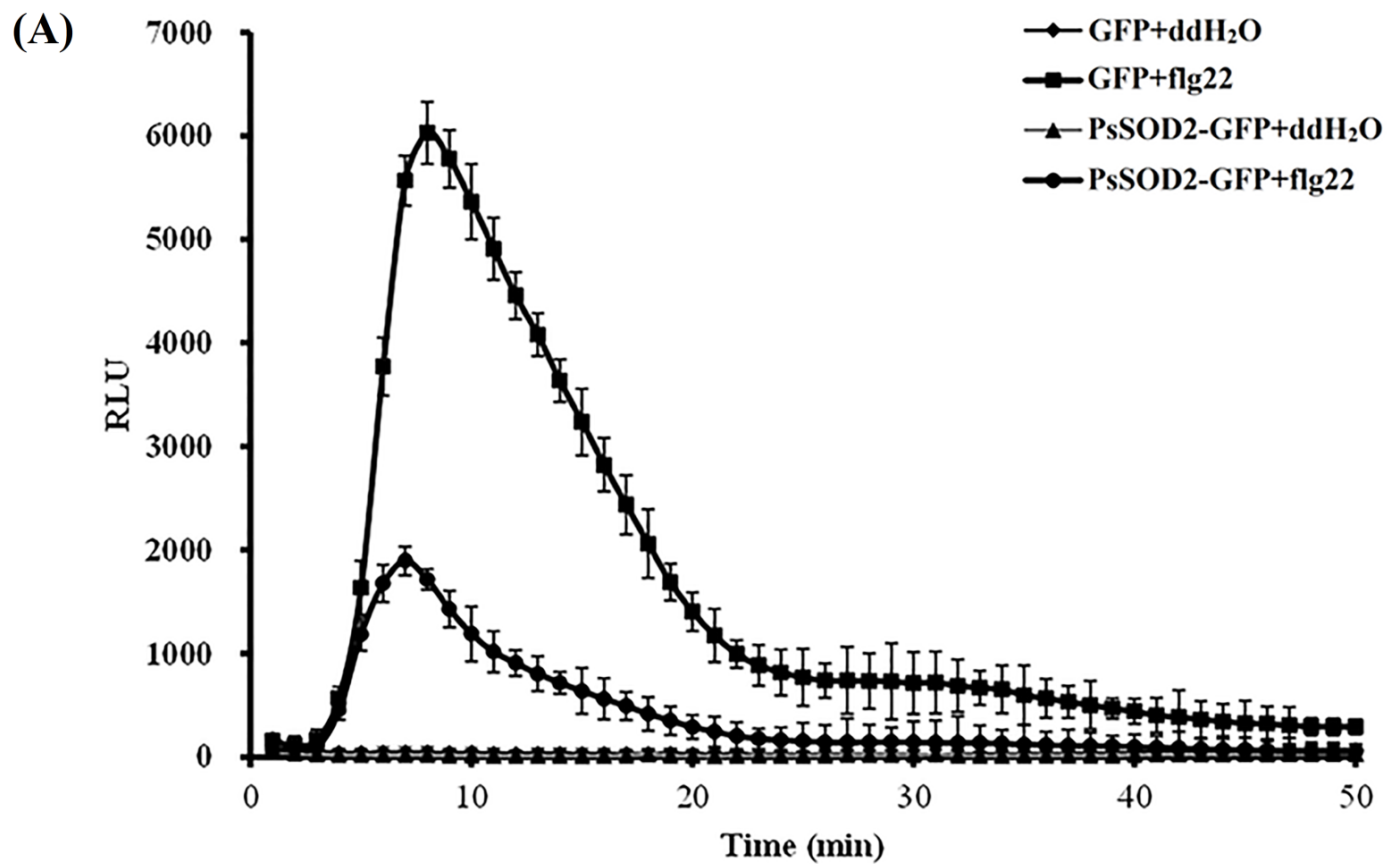


Fig. 5



(B)

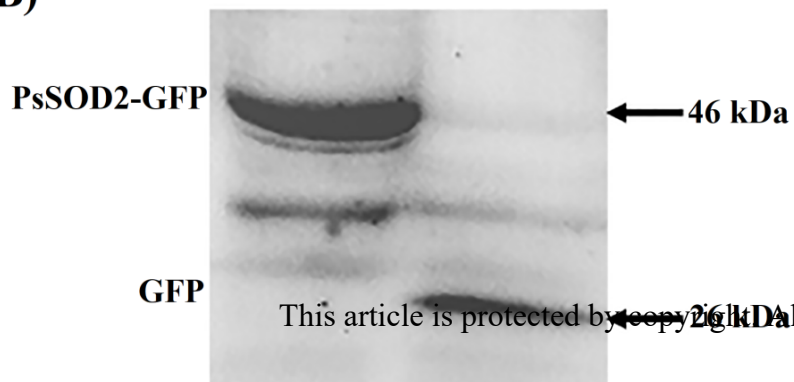


Fig. 6

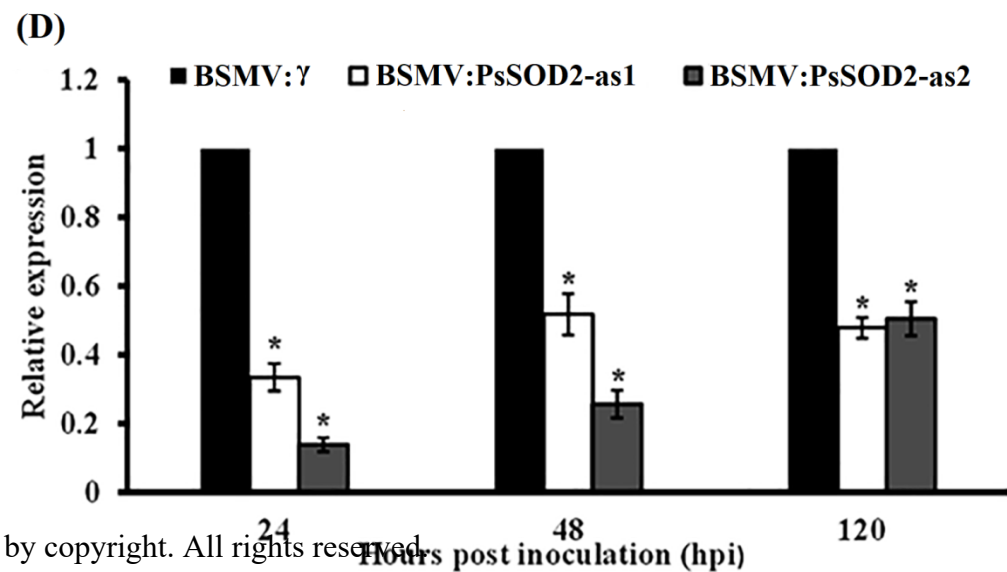
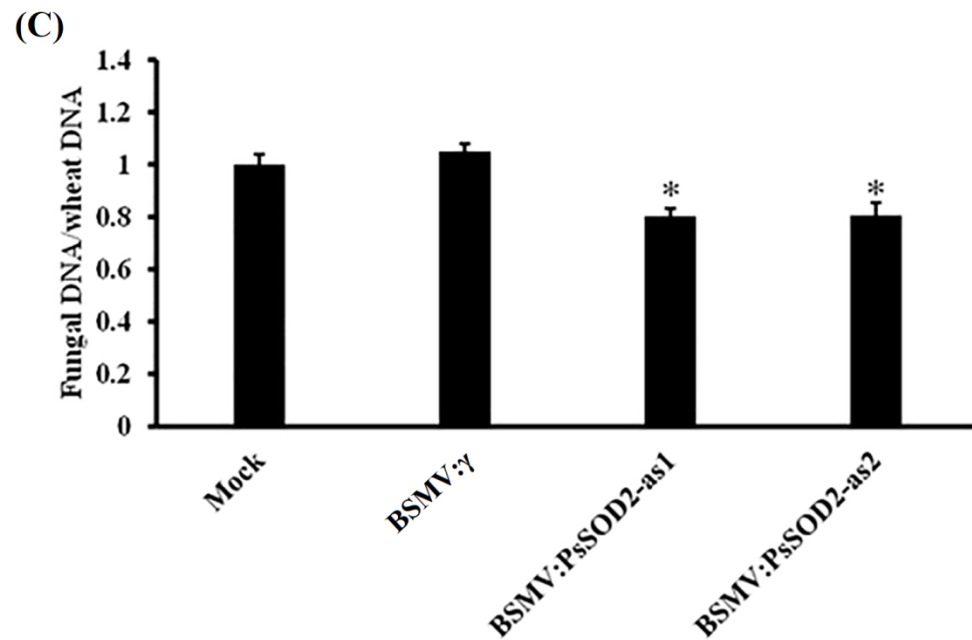
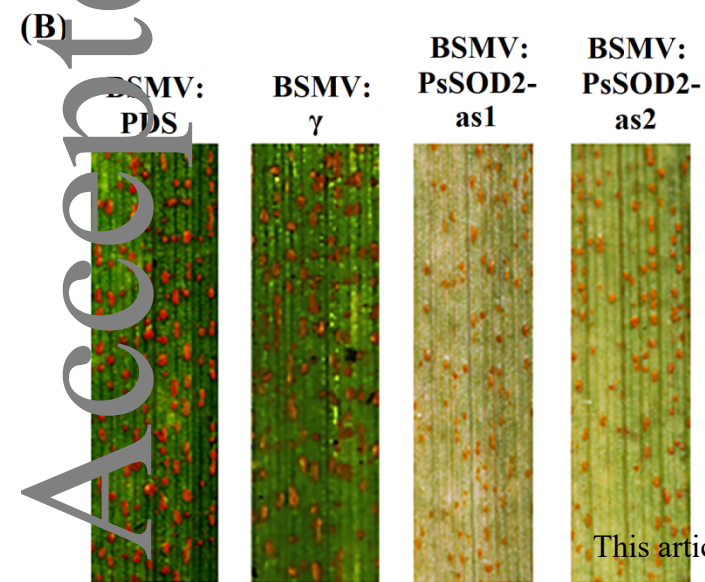
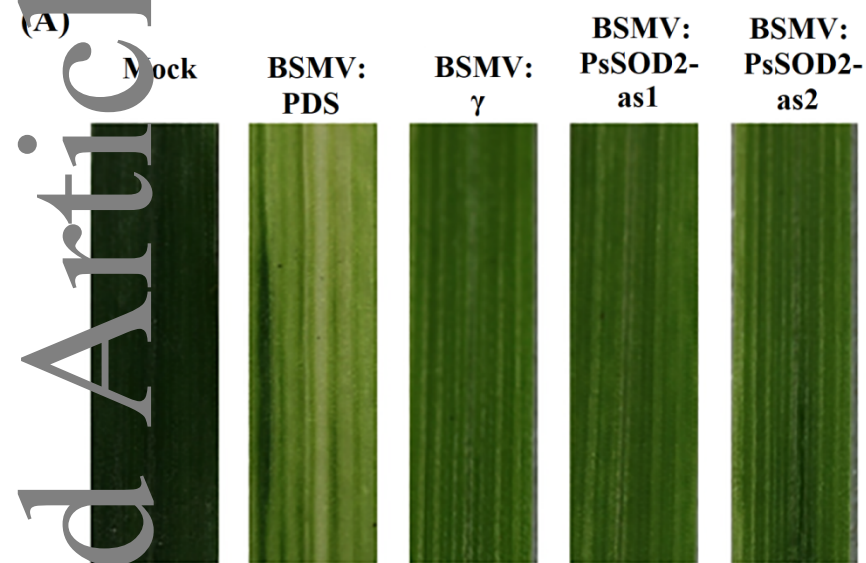


Fig. 7

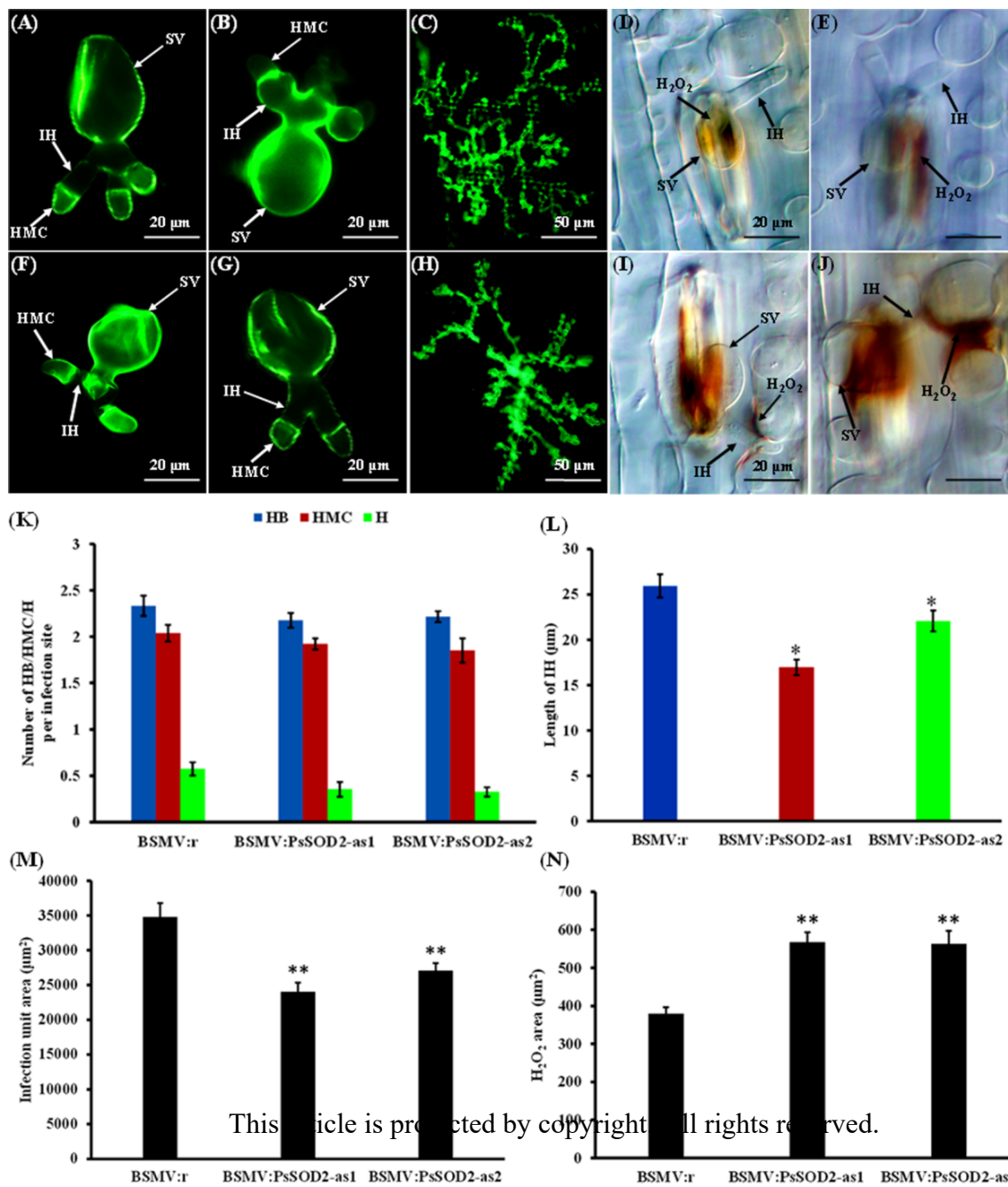


Fig. 8

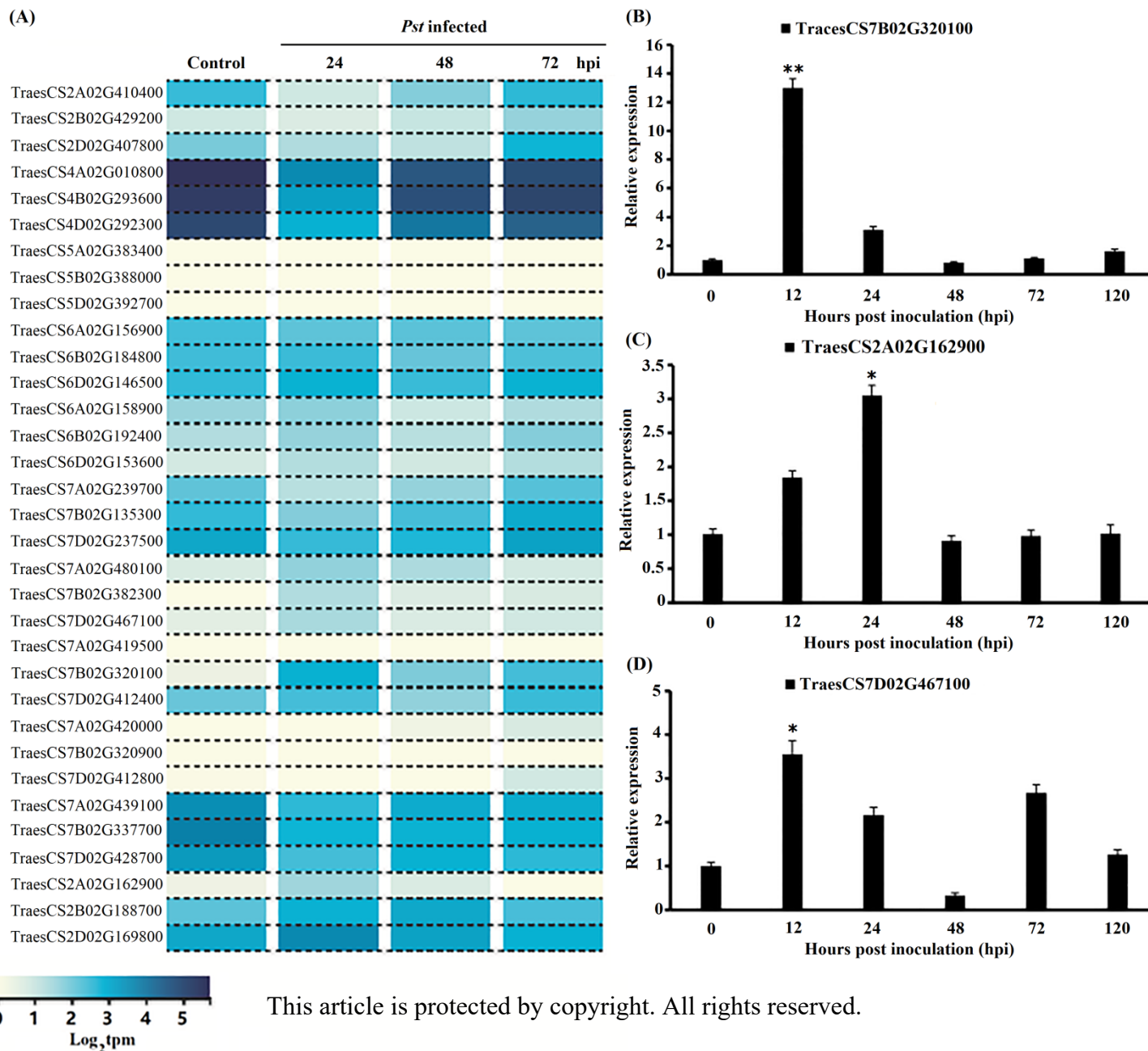


Fig. 9

